








# Endothelial Piezo1 channel mediates mechano-feedback control of brain blood flow

Received: 4 March 2024

Accepted: 25 September 2024

Published online: 07 October 2024

 Check for updates

Xin Rui Lim <sup>1,2,9</sup>, Mohammad M. Abd-Alhaseeb <sup>1,2,9</sup>, Michael Ippolito <sup>1,2</sup>, Masayo Koide<sup>1,2</sup>, Amanda J. Senatore<sup>1,2</sup>, Curtis Plante<sup>1,2</sup>, Ashwini Hariharan<sup>3,4</sup>, Nick Weir<sup>3,4</sup>, Thomas A. Longden <sup>3,4</sup>, Kathryn A. Laprade<sup>5</sup>, James M. Stafford<sup>5</sup>, Dorothea Ziemens<sup>6,7</sup>, Markus Schwaninger <sup>6,7</sup>, Jan Wenzel <sup>6,7</sup>, Dmitry D. Postnov<sup>8</sup> & Osama F. Harraz <sup>1,2</sup> ✉

Hyperemia in response to neural activity is essential for brain health. A hyperemic response delivers O<sub>2</sub> and nutrients, clears metabolic waste, and concomitantly exposes cerebrovascular endothelial cells to hemodynamic forces. While neurovascular research has primarily centered on the front end of hyperemia—neuronal activity-to-vascular response—the mechanical consequences of hyperemia have gone largely unexplored. Piezo1 is an endothelial mechanosensor that senses hyperemia-associated forces. Using genetic mouse models and pharmacologic approaches to manipulate endothelial Piezo1 function, we evaluated its role in blood flow control and whether it impacts cognition. We provide evidence of a built-in brake system that sculpts hyperemia, and specifically show that Piezo1 activation triggers a mechano-feedback system that promotes blood flow recovery to baseline. Further, genetic Piezo1 modification led to deficits in complementary memory tasks. Collectively, our findings establish a role for endothelial Piezo1 in cerebral blood flow regulation and a role in its behavioral sequelae.

Neurons in the brain rely on an on-demand energy delivery strategy in which active neurons trigger signaling to the vasculature to locally elevate blood flow—a phenomenon referred to as functional hyperemia (FH)<sup>1,2</sup>. The increase in cerebral blood flow (CBF) during FH satisfies the metabolic demands of active neurons by delivering O<sub>2</sub> and nutrients and clearing metabolic waste. The impact of hyperemia, however, extends considerably beyond the provision of energy; hyperemia is implicated in temperature regulation and

cerebrospinal fluid dynamics<sup>3,4</sup>. The hyperemic response is further associated with increases in frictional forces imposed by blood flow onto endothelial cells (ECs) of cerebral arterioles and capillaries<sup>1,5,6</sup>. While neurovascular research has primarily centered on the front end of the FH process (i.e., neuronal activity-to-vascular response), the back end—mechanical consequences of FH and mechanisms that reset blood flow after hyperemic responses—has gone largely unexplored.

<sup>1</sup>Department of Pharmacology, Larner College of Medicine, University of Vermont, Burlington, VT, USA. <sup>2</sup>Vermont Center for Cardiovascular and Brain Health, University of Vermont, Burlington, VT, USA. <sup>3</sup>Department of Physiology, School of Medicine, University of Maryland, Baltimore, MD, USA. <sup>4</sup>Laboratory of Neurovascular Interactions, Center for Biomedical Engineering and Technology, School of Medicine, University of Maryland, Baltimore, MD, USA. <sup>5</sup>Department of Neurological Sciences, Larner College of Medicine, University of Vermont, Burlington, VT, USA. <sup>6</sup>Institute of Experimental and Clinical Pharmacology and Toxicology, Center of Brain, Behavior and Metabolism (CBBM), University of Lübeck, Lübeck, Germany. <sup>7</sup>German Research Centre for Cardiovascular Research (DZHK), partner site Hamburg/Lübeck/Kiel, Lübeck, Germany. <sup>8</sup>Center of Functionally Integrative Neuroscience, Department of Clinical Medicine, Aarhus University, Aarhus 8200, Denmark. <sup>9</sup>These authors contributed equally: Xin Rui Lim, Mohammad M. Abd-Alhaseeb.

✉ e-mail: [Osama.Harraz@uvm.edu](mailto:Osama.Harraz@uvm.edu)

A neuronal action potential is initiated by depolarization due to  $\text{Na}^+$  channel activation. The change in neuronal membrane potential ( $V_m$ ) due to  $\text{Na}^+$  influx subsequently activates voltage-activated  $\text{K}^+$  channels leading to  $\text{K}^+$  efflux, increased extracellular  $\text{K}^+$  concentration, and neuronal membrane repolarization<sup>7</sup>. Not only does this elevated extracellular  $\text{K}^+$  concentration reset neuronal  $V_m$  during cortical activity, it also dramatically enhances nearby vascular  $\text{K}^+$  conductance via the activation of inwardly rectifying  $\text{K}^+$  Kir2.1 channel in ECs<sup>8</sup>. The subsequent EC hyperpolarization propagates to electrically coupled ECs and smooth muscle cells (SMCs), leading to vasodilation, and then to hyperemia, as evidenced by the critical involvement of EC Kir2.1 channels in FH<sup>8,9</sup>. In addition to  $\text{K}^+$ , neuronally derived vasodilators, such as nitric oxide (NO), adenosine, and prostaglandin E2 signal to vascular cells to ultimately trigger hyperemia<sup>10–13</sup>. The latter neurovascular coupling agents are released outside the brain vasculature, thus affecting vascular signaling and CBF. It is not fully understood, however, how hyperemia-associated forces within the cerebrovasculature could themselves affect CBF.

We recently discovered that intravascular forces, like those generated during FH, activate the mechanosensor Piezo1 in the central nervous system (CNS) endothelium<sup>14</sup>. The Piezo1 channel is permeable to  $\text{Ca}^{2+}$  and  $\text{Na}^+$ , and we demonstrated that mechanical stimulation triggers Piezo1-mediated cationic currents and  $\text{Ca}^{2+}$  signals in ECs<sup>14–16</sup>. Cation influx canonically depolarizes cells, and it has been shown that flow forces depolarize vascular ECs in a Piezo1-dependent manner<sup>17,18</sup>. The electrical coupling between ECs and the surrounding mural cells (e.g., SMCs) presumably allows the spread of Piezo1-mediated electrical signals from ECs to SMCs<sup>17,19,20</sup>. While our previous observations implicated Piezo1 as a mechanosensor in the brain vasculature, the functional consequences of Piezo1 activation on CBF control remain unknown.

Here, we demonstrate that endothelial Piezo1 channels have a major role in CBF control. Enhancing Piezo1 function pharmacologically or genetically in ECs suppresses hyperemic responses and accelerates blood flow recovery to baseline at the conclusion of hyperemic events. We show that Piezo1 activation is the crux of a mechano-feedback system that promotes blood flow recovery to baseline, suggesting that EC Piezo1 channels serve as a built-in brake system that sculpts not only the amplitude but also the kinetics of the hyperemic response. EC Piezo1 function modification translates to altered performance in behavioral tests suggesting a potential link between Piezo1 impact on neurovascular coupling and cognition. Our findings collectively establish an important role for cerebrovascular Piezo1 channel in brain blood flow regulation and its behavioral sequelae.

## Results

### Piezo1 activation suppresses brain cortex hyperemia

We recently showed that Piezo1 is functionally expressed in ECs of the CNS. Using electrophysiology and  $\text{Ca}^{2+}$  imaging, we observed Piezo1-mediated inward cation currents and  $\text{Ca}^{2+}$  signals that were mechanically or pharmacologically triggered<sup>14</sup>. To study the impact of Piezo1 function on CBF, we set out to study the impact of pharmacological Piezo1 activation on FH. Wildtype C57BL/6J mice were anesthetized and fitted with a cranial window above the somatosensory cortex, and a laser Doppler flowmetry probe was placed over the barrel cortex<sup>9</sup>. Contralateral whiskers were mechanically stimulated (4 Hz), and CBF was monitored before and after the cortical application of the Piezo1 activator Yoda1 (30  $\mu\text{M}$ ) (Fig. 1a, b). FH was reduced from  $25.5 \pm 2.5\%$  to  $17.2 \pm 0.8\%$  after Yoda1 application (Fig. 1c, d), but there was no change in baseline CBF or blood pressure (Fig. 1e, f). In distinction, vehicle application failed to affect FH or blood pressure (Fig. 1g, h). To further support these findings, we used two-photon laser scanning microscopy to test whether Yoda1 attenuates arteriolar dilation in response to whisker stimulation (Fig. 1i). Penetrating arterioles in the barrel

cortex were visualized in anesthetized C57BL/6J mice. Whisker stimulation evoked vasodilation was significantly reduced after Yoda1 application (from  $15.2 \pm 3.3\%$  to  $5.5 \pm 0.7\%$ , Fig. 1j, k), despite no change in baseline arteriolar diameter before ( $7.2 \pm 0.7 \mu\text{m}$ ) and after ( $7.6 \pm 0.5 \mu\text{m}$ ) Yoda1 application. These observations collectively suggested that Piezo1 suppresses FH.

### Enhanced endothelial Piezo1 activity is associated with impaired FH

Targeting Piezo1 using an activator applied to the surface of the brain cortex suppressed FH (Fig. 1). Within the brain, the primary cell type with the highest expression levels of Piezo1 is ECs across the vascular network (in arteries, capillaries, veins), as shown by RNA transcriptomic studies<sup>21,22</sup>. Recent studies have additionally demonstrated non-vascular functional expression<sup>23,24</sup>. As cortical Yoda1 application could lead to non-specific effects, and to specifically target endothelial Piezo1, we genetically engineered a gain-of-function (GOF) mouse model in which Piezo1 function is enhanced only in ECs. Tamoxifen-inducible GOF mice were developed by crossing *Cdh5-CreER*<sup>T2</sup> (EC-specific inducible Cre recombinase) mice with a knock-in mouse in which floxed exons 45–51 are followed by a mutant Piezo1 copy like that in human xerocytosis patients<sup>25</sup>. This mutant Piezo1 channel is characterized by slower inactivation kinetics and an increase in cation influx when activated<sup>25,26</sup>. Cre-positive mice were designated ‘GOF’ (Piezo1<sup>cx/cx</sup>; *Cdh5-Cre*+) and littermate Cre-negative mice (Piezo1<sup>cx/cx</sup>; *Cdh5-Cre*-) were used as controls (Fig. 2a). We first tested whether Piezo1 activity is enhanced in ECs from GOF mice using freshly isolated ECs and patch clamp electrophysiology<sup>14</sup>. Single channel open probability was significantly higher in ECs from GOF mice compared with controls when recorded in the absence or presence of Yoda1, validating this mouse model as an EC-specific Piezo1 GOF (Fig. 2b, c). Next, we measured hyperemic responses to whisker stimulation in anesthetized GOF mice (with urethane and  $\alpha$ -chloralose) using laser speckle contrast imaging (LSCI) (Fig. 2d, e). To minimize the impact on intracranial pressure—which could impact mechanical forces generated during FH—all LSCI experiments employed skull thinning rather than craniotomy. The whiskers were stimulated for 5 or 30 s—shorter durations, than those in Fig. 1—as neurovascular coupling normally triggers hyperemia within a few seconds<sup>1,2,5</sup>. Whisker stimulation using air puffs (5 Hz) evoked hyperemia in the contralateral barrel cortex. Compared with controls, the maximum hyperemic responses in GOF mice were reduced from  $14.7 \pm 1.6\%$  to  $9.7 \pm 0.7\%$  (30 s stimulation) and from  $10.3 \pm 1\%$  to  $7.4 \pm 0.6\%$  (5 s stimulation) (Fig. 2f–i). Baseline hemisphere CBF was similar between GOF mice and controls (Fig. S1).

Structural changes in the cerebral vasculature could lead to a defect in FH. To test whether cerebrovascular structural changes in GOF mice underlie the impaired CBF responses, we stained brain slices from the cortex and hippocampus for ECs and basement membrane, as we have done before<sup>27</sup>. Vascular density was similar between GOF and control mice (Fig. 2j, k). Thin ( $<4 \mu\text{m}$ ) EC-negative and basement membrane-positive structures—known as string vessels, which are linked to poor CBF and brain ischemia<sup>28,29</sup>—were not different in Piezo1<sup>cx/cx</sup>; *Cdh5-Cre* mice (Fig. 2j, k). Lengths and diameters of  $\alpha$ -smooth muscle actin ( $\alpha$ -SMA)-positive vessels (i.e., arteries, arterioles, and transitional segments) and pericyte coverage (PDGFR $\beta$ -positive) were similar in the cortex or the hippocampus of Piezo1<sup>cx/cx</sup>; *Cdh5-Cre* mice and controls (Fig. S2, S3). Further, immunostaining for markers of neurons (NeuN or neurofilament 200), astrocytes (GFAP), or microglia (Iba1) revealed no differences in mice with mutant Piezo1 channels (Fig. S4, S5, S6, S7). In conclusion, targeting ECs to enhance Piezo1 function inhibited FH. Our robust results across multiple distinct paradigms (cranial window vs. thinned skull, and different-length stimulations) strengthen the conclusion that Piezo1 activation curtails FH, without altering cerebrovascular structure.

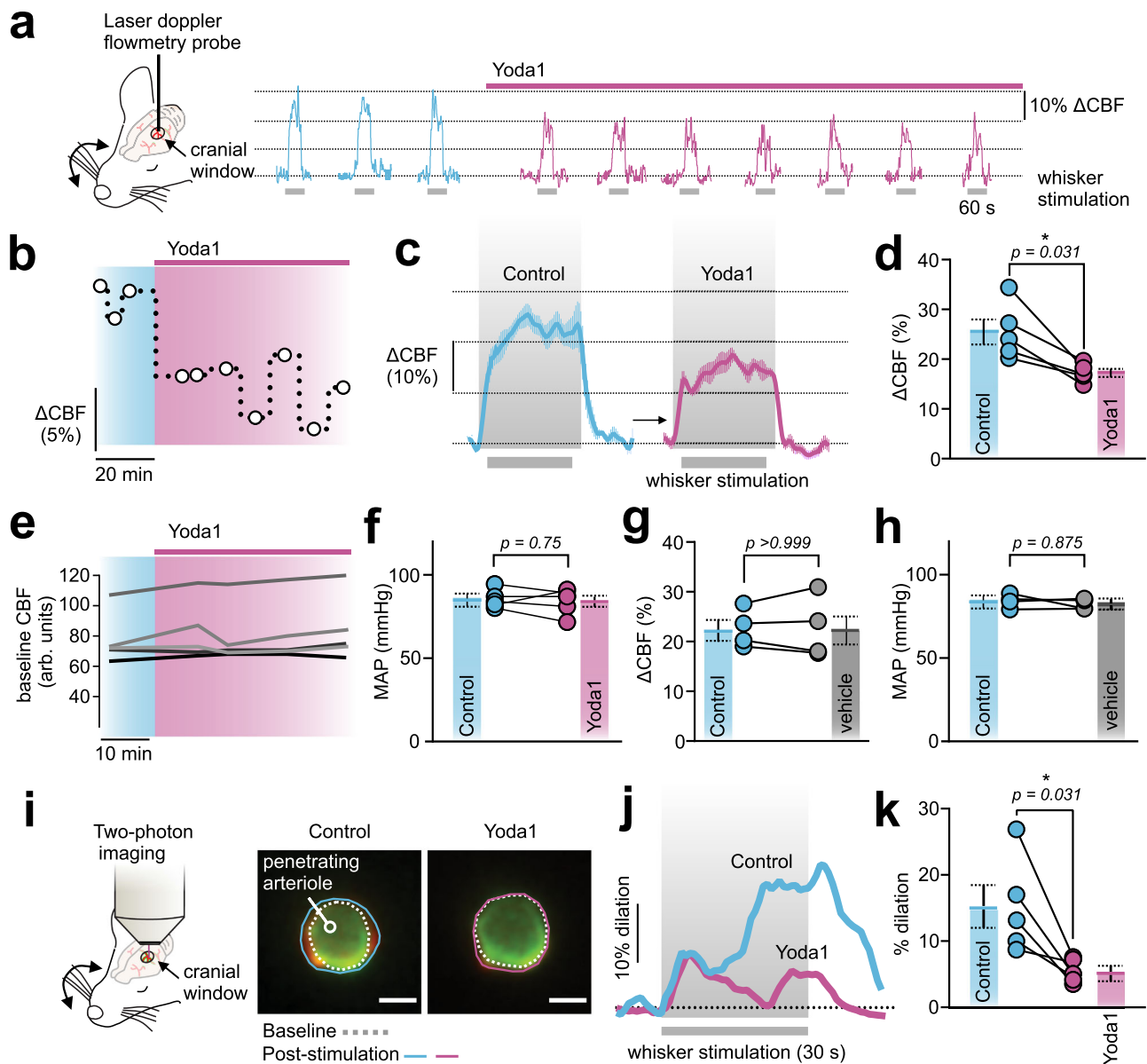


**Fig. 1 | Piezo1 activation inhibits brain functional hyperemia (FH).** **a** Whisker stimulation experimental scheme (*left*) and representative traces showing whisker stimulation-induced changes in CBF ( $\Delta$ CBF) in the contralateral somatosensory barrel cortex of a C57BL/6J mouse before and after Yoda1 (30  $\mu$ M) application onto a cranial window. **b** Time course reflects the change in FH amplitude ( $\Delta$ CBF) from the experiment in **a** after the application of Yoda1. Each circle denotes one stimulation. **c** Average waveforms of whisker stimulation-induced CBF changes in the absence and presence of Yoda1 ( $n = 5$  mice). **d** Summary data showing the effect of Yoda1 on CBF increases ( $n = 5$  mice). **e** Baseline CBF in arbitrary units (arb. units) before and after Yoda1 application. **f** Impact of cortical application of Yoda1 on mean arterial blood pressure (MAP) measured using a femoral artery catheter ( $n = 5$  mice). **g, h** Vehicle application had no effect on CBF increases or MAP ( $n = 4$

mice). **i** Two-photon laser scanning microscopy experimental scheme and images of penetrating arteriolar diameter before (*dotted*) and after (*solid*) whisker-stimulation evoked arteriolar dilation. Scale bar = 5  $\mu$ m. In a control mouse, whisker stimulation evoked a large increase in arteriolar diameter that was absent in the presence of Yoda1 (cortical, 30  $\mu$ M). The experiment was repeated independently in 5 C57BL/6J mice (summarized in **k**). **j** Representative traces of arteriolar dilation in response to a 30 s whisker stimulation before and after Yoda1. **k** Summary of arteriolar responses to the described stimuli ( $n = 5$  mice). Wilcoxon statistical test was used in **d-h** (one-sided in **d** and two-sided in **f-h**) and paired Student's *t*-test (two-sided) in **k** ( $*P < 0.05$ ). All error bars are standard error of the mean (SEM). Data in **c, d, f, g, h, k** are presented as mean values  $\pm$  SEM. Source data are provided as a Source Data file.

### Functional hyperemia kinetics are dictated by Piezo1 activity

Our observations suggest that pharmacological (Fig. 1) or genetic (Fig. 2) enhancement of Piezo1 activity suppressed blood flow increase during FH. Therefore, we hypothesized that endothelial Piezo1 channels act as a built-in brake system for hyperemia: Piezo1 senses hyperemic forces and engages a mechano-feedback system that attenuates (or short-circuits) hyperpolarization-mediated<sup>8</sup> increases in CBF. This hypothesis can be posed as an analogy to the neuronal action potential, where  $\text{Na}^+$  channel activation depolarizes neurons. The latter

depolarization is, itself, the trigger for neuronal  $\text{K}^+$  channel activation, which acts as a built-in brake system to repolarize neurons to resting  $V_m$ <sup>7</sup>. Within the vasculature, endothelial hyperpolarization evokes hyperemia<sup>8</sup>, which could in turn engage Piezo1 (the built-in brakes) to depolarize ECs and terminate hyperemia (Fig. 3a). A critical condition that needs to be met in this hypothesis is that Piezo1 activation depolarizes brain ECs. Indeed, sharp electrode impalement of freshly isolated brain ECs demonstrated that Yoda1 robustly depolarized ECs from  $-37.6 \pm 1.8$  mV to  $-29.1 \pm 1.2$  mV (Fig. 3b, c), consistent with a

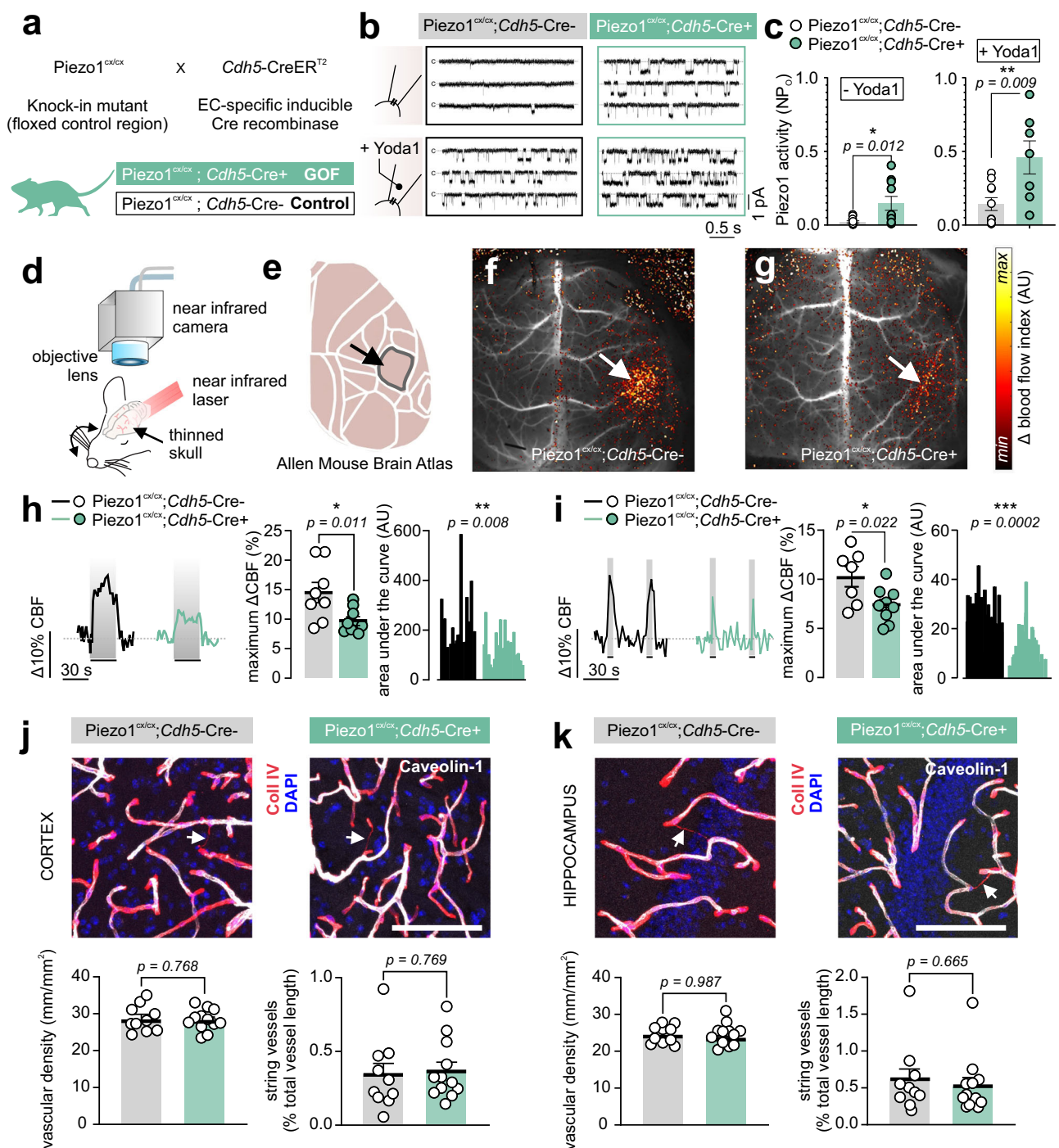


**Fig. 2 | EC-specific Piezo1 gain-of-function (GOF) mice demonstrate impaired functional hyperemia.** **a** Crossbreeding scheme used to generate inducible, EC-specific Piezo1-GOF mice. Tamoxifen-treated Cre<sup>+</sup> mice are used as GOF, and littermate Cre<sup>-</sup> mice are the control. **b** Representative traces of Piezo1 currents recorded from freshly isolated ECs from the somatosensory cortices of control and GOF mice. The cell-attached configuration was used, where EC patches were held at -50 mV in the absence or presence of Yoda1 (5 μM) in the pipette solution. **c** Denotes closed channel. **c** Averaged data of the open probability (NP<sub>o</sub>) of Piezo1 in the absence (n = 11 ECs/6 control; 10 ECs/4 GOF mice) or presence of Yoda1 (n = 10 ECs/6 control; 7 ECs/4 GOF mice). **d** Schematic of the LSCI setup for imaging blood flow through a thinned skull. **(e)** The Allen mouse brain atlas highlighting the somatosensory barrel cortex. **f, g** Differential maps of blood flow responses in a control (**f**) and a GOF (**g**) mouse. Whisker stimulation using air puffs (5 Hz, 30 s) evoked hyperemia in the contralateral somatosensory cortex (arrows). **h** Representative traces and summary data of the hyperemic response to 30 s-whisker stimulations in

control (n = 8) and GOF (n = 9) mice. Right: area under the curve analyses (n = 19 whisker stimulations/6 control; 20 stimulations/8 GOF mice). **i** Representative responses and scatter plots of FH evoked by 5 s air puffs (n = 7 control, n = 9 GOF mice). Area under the curve analysis was calculated from 41 and 43 stimulations from 7 control and 9 GOF mice, respectively. **j** Representative images demonstrating the staining of ECs (caveolin-1), basement membranes (collagen IV), and nuclei (DAPI) in brain slices of the cortex of GOF and control mice. Scale bar: 100 μm. Vascular densities and string vessel densities in Piezo1<sup>lox/lox</sup>; Cdh5-Cre+ (n = 12) and control (n = 10) mice. **k** Representative images and averaged data as in **j** from brain slices of the hippocampus of Piezo1<sup>lox/lox</sup>; Cdh5-Cre+ (n = 12) and control (n = 10) mice. All statistical tests were unpaired Student's t test (two-sided, \*P < 0.05, \*\*P < 0.01, \*\*\*P < 0.001). All error bars are SEM. Scatter plot data in **c, h, i, j, k** are presented as mean ± SEM. Area under the curve data in **h** and **i** are presented as histograms. Source data are provided as a Source Data file.

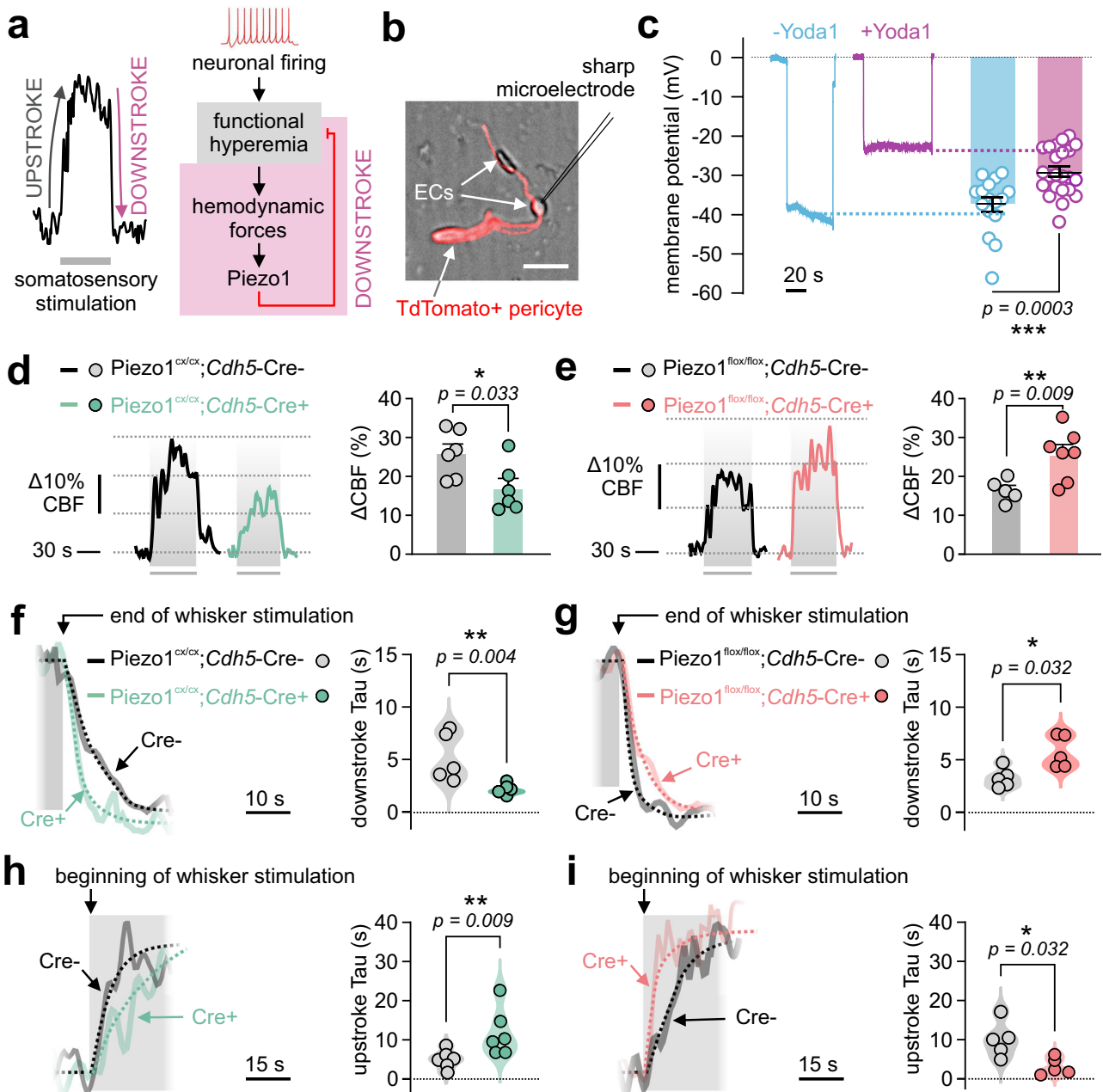


**Fig. 3 | Endothelial Piezo1 shapes the functional hyperemic response.** **a Left:** Example FH response to whisker stimulation showing the increase in CBF shortly after the stimulus starts (upstroke) and the return to baseline at the end of the stimulation (downstroke). **Right:** A schematic showing that neuronal activity increases blood flow (FH), and the resulting change in forces activates cationic influx by opening Piezo1 channels, thus acting as a mechano-feedback system to attenuate FH. **b** Experimental setup illustrating impalement of a freshly isolated brain EC using a sharp microelectrode. ECs were obtained from a *Pdgfrb-Cre-TdTomato* mouse, where pericytes are TdTomato+. Scale bar = 10  $\mu\text{m}$ . **c** Traces and summary data of  $V_m$  measurements showing the effect of Yoda1 (5  $\mu\text{M}$ ) on endothelial  $V_m$  (-Yoda1 [ $n = 16$  ECs/5 mice]; +Yoda1 [ $n = 23$  ECs/4 mice]). **d, e** Representative traces and scatter plots of functional hyperemia responses to whisker stimulations in *Piezo1<sup>cx/cx</sup>; Cdh5-Cre-* (GOF) and *Piezo1<sup>lox/lox</sup>; Cdh5-Cre+* (knockout) mice, and their respective controls (**d**:  $n = 6$  GOF, 6 controls; **e**:  $n = 7$  knockout, 5

controls). **f** Representative traces and plateau-followed-by-exponential fittings (dotted) to obtain time constant for downstroke (Tau), in a control mouse and a GOF mouse. **Right:** Scatter plot of downstroke Tau values in control ( $n = 5$ ) and GOF ( $n = 6$ ) mice. **g** Similar to **f** in knockout and control mice ( $n = 5$  each). **h** Representative traces and plateau-followed-by-exponential fittings (dotted) to obtain upstroke Tau values in a control mouse and a GOF mouse. **Right:** Scatter plot of upstroke Tau values in control and GOF ( $n = 6$  mice each). **i** Representative traces and averaged data of upstroke Tau in control and knockout mice ( $n = 5$  mice each). FH responses were measured through a cranial window using laser Doppler flowmetry. Statistical tests were unpaired Student's t test (two-sided, **c**), and Mann-Whitney test (one-sided in **d-e**, two-sided in **f-i**; \* $P < 0.05$ , \*\* $P < 0.01$ , \*\*\* $P < 0.001$ ). Error bars in **c, d** and **e** are SEM. Data in **c, d, e** are presented as mean values  $\pm$  SEM, and data in **f, g, h, i** are presented as violin scatter plots. Source data are provided as a Source Data file.

depolarizing role for endothelial Piezo1 in the cerebral circulation, as has been shown in peripheral ECs<sup>17,18</sup>.

If Piezo1 serves a mechano-feedback role, it is conceivable that modulating its function will affect the waveform of FH. To use motor analogies, we speculated that Piezo1 activity could impact the maximal

hyperemia response (i.e. engine capacity), the upstroke (i.e. acceleration), and blood flow recovery kinetics when the stimulus ceases (i.e. braking). We used laser Doppler flowmetry and observed that whisker stimulation led to decreased hyperemic responses in *Piezo1<sup>cx/cx</sup>; Cdh5-Cre+* mice compared to their controls (Fig. 3d).

On the other hand, we engineered an inducible, EC-specific Piezo1 knockout (Piezo1<sup>lox/lox</sup>; *Cdh5*-Cre+) mouse model<sup>14</sup> in which somatosensory stimulations led to enhanced responses (Fig. 3e), consistent with a role for Piezo1 as a negative feedback. Notably, Piezo1<sup>cx/cx</sup> and Piezo1<sup>lox/lox</sup> mice have different genetic backgrounds that are known to alter Piezo1-mediated Ca<sup>2+</sup> signaling in Cre- controls<sup>30</sup>. Further, these backgrounds demonstrate key differences in CBF dynamics<sup>31,32</sup>. Given the differences observed in CBF across control (Cre-) mice here (Fig. 3d, e) and the differences seen in Piezo1<sup>cx/cx</sup> and Piezo1<sup>lox/lox</sup> Cre- and Cre+ without tamoxifen treatment (i.e., no induction; Fig. S8), hyperemic responses were only compared to controls of the same genetic background in all analyses.

Next, kinetic analyses were performed for the decline phase reflecting the return of CBF back to baseline levels (referred to as downstroke), with the anticipation that enhancing Piezo1 activity, or its loss will accelerate or decelerate the downstroke, respectively. We calculated time constants (Tau) of the exponential fittings of the decrease of blood flow from maximal response to baseline. As expected, time constants of the downstroke were lower in GOF mice compared to their controls (Fig. 3f), indicating faster blood flow recovery. Piezo1<sup>lox/lox</sup>; *Cdh5*-Cre+ mice, in contrast, demonstrated higher time constants than their controls indicative of a slower recovery (Fig. 3g). Paired analyses of downstroke time constants revealed that chemical activation of Piezo1 (30  $\mu$ M Yoda1, cortical perfusion) accelerated the FH downstroke and the return of arteriolar diameter to baseline in wildtype mice (Fig. S9). Lastly, analyses of the rising phase of hyperemia (upstroke) demonstrated that enhanced Piezo1 activity (GOF or Yoda1) slowed down the increase in blood flow (Fig. 3h, S9, S10), and the opposite was observed in knockout mice (Fig. 3i). These findings collectively support a mechanism by which Piezo1 acts as a negative feedback system for FH during somatosensory stimulation.

### A human Piezo1 GOF mutation in brain ECs impairs hyperemic responses

Introducing a GOF mutant Piezo1 channel in ECs throughout the vasculature (i.e., pan-endothelial) impaired FH (Figs. 2, 3). It is possible that altered peripheral vascular Piezo1 function in GOF mice contributes to the observed impact on CBF, considering that previous studies demonstrated a role for EC Piezo1 in the periphery in modulating vascular diameter<sup>17,33</sup>. To ascertain whether enhanced EC Piezo1 function in the CNS alone is sufficient and responsible for CBF impairment, we developed a mouse model in which only the brain endothelial Piezo1 is replaced with a mutant GOF channel. Brain EC-specific GOF animals were generated by crossing the transgenic brain-EC-specific Cre-recombinase *Slo1c1-CreER*<sup>T2</sup> strain<sup>34,35</sup> with floxed knock-in mice with a mutant Piezo1 copy (Fig. 4a). Using LSCI, we observed that Piezo1<sup>cx/cx</sup>; *Slo1c1*-Cre+ mice displayed attenuated hyperemic responses to whisker stimulation. Air puff stimulation of whiskers (5 or 30 s, 5 Hz) evoked hyperemic responses with maximal increases that were reduced in Piezo1<sup>cx/cx</sup>; *Slo1c1*-Cre+ mice from 12.6 $\pm$ 1.6% to 6.9 $\pm$ 1.0% (30 s stimulation) or from 7.0 $\pm$ 0.7% to 4.5 $\pm$ 0.5% (5 s stimulation) (Fig. 4c–f). Similar suppression was observed when whiskers were stimulated at 3–4 Hz manually (from 11.7% to 6.6%) or using a motor actuator (from 10.3% to 6.4%) (Fig. 4g). Calibrated hemisphere baseline blood flow was similar between Piezo1<sup>cx/cx</sup>; *Slo1c1*-Cre+ and control mice (Fig. 4h).

### Recovery from CO<sub>2</sub>-induced hyperemia is governed by Piezo1 activity

Our observations suggest that Piezo1 activity acts as a negative feedback system to facilitate the return of increased blood flow during FH back to baseline levels. These findings were evident during whisker stimulation, demonstrating that EC-Piezo1 serves as a brake system to counteract hyperemia elicited by increased neuronal firing. It is

unknown, however, whether a mechano-feedback role for Piezo1 is limited to hyperemia evoked by somatosensory stimulation, or if the feedback function of Piezo1 is more universal and engaged during other hyperemic responses. To test the latter possibility, we set out to study CO<sub>2</sub>-induced hyperemia<sup>34,36</sup> in Piezo1<sup>cx/cx</sup>; *Slo1c1*-Cre+ mice and their controls. Hypercapnia (elevated CO<sub>2</sub>) was evoked in anesthetized mice (urethane and  $\alpha$ -chloralose) by elevating CO<sub>2</sub> in the inhaled air to 10% while monitoring CBF. Following a 5 min baseline, CO<sub>2</sub> evoked hyperemia of similar maximal amplitude in control (124.6% increase) and Piezo1<sup>cx/cx</sup>; *Slo1c1*-Cre+ mice (117.4%) (Fig. 5a–c). The kinetics of CBF increases were similar in both groups (Fig. S11). However, CBF recovered to baseline significantly faster in GOF mice. Averaged time constants (Tau) for recovery were 192s (control) and 91s (Piezo1<sup>cx/cx</sup>; *Slo1c1*-Cre+). Along the same lines, area under the curve analysis showed less blood flow in Piezo1<sup>cx/cx</sup>; *Slo1c1*-Cre+ mice during the recovery phase. Recovery started sooner and returned to baseline faster in GOF mice, indicative of a more rapid return to baseline when Piezo1 activity is augmented (Fig. 5d–h). We further engineered mice in which Piezo1 channels were knocked out in brain ECs. Piezo1<sup>lox/lox</sup>; *Slo1c1*-Cre+ mice displayed robust CBF increases to CO<sub>2</sub> that were comparable to those in Cre-negative control mice (Fig. 5i, j). Recovery from hypercapnia-evoked hyperemia was slower in brain EC Piezo1 knockout mice (averaged Tau: 133s vs. 87s in controls), consistent with compromised CBF recovery due to the lack of Piezo1 function (Fig. 5k–o). Comparisons were only made to respective controls due to genetic background differences (Fig. S12). We expected that—like FH—hypercapnia-induced hyperemia will be different in GOF mice in both magnitude and kinetics, but we observed consistent differences only during recovery. This could be attributed to the huge temporal variability between stimulations (5–30 s versus 900 s), and the distinct mechanisms underlying different hyperemic responses<sup>36,37</sup>. Together, our observations demonstrate that Piezo1 dictates CBF recovery to baseline at the end of hyperemia, whether evoked through somatosensory (Figs. 1–4) or hypercapnic (Fig. 5) stimulations.

### Mice with endothelial Piezo1 GOF display deficits in memory

Vascular dysfunction makes major contributions to the severity and progression of several forms of dementia. Deficits in CBF are reported in neurodegenerative and small vessel diseases, and the degree of blood flow deficits correlates with the severity of cognitive dysfunction and memory loss<sup>38–42</sup>, consistent with neurovascular coupling and FH being critical for learning and memory<sup>43</sup>. Because we observed a decline in FH in mice where Piezo1 activity was enhanced (Figs. 1–5), we hypothesized that GOF mice display altered cognitive performance. To directly assess cognition, we utilized two tests of memory—the novel object recognition (NOR), and the spontaneous alternation T-maze, tasks sensitive to alterations in neurovascular coupling and affected in neurological disease models<sup>43,44</sup>. Both tests assess cognition, with the NOR test reflecting long-term recognition memory, and the spontaneous alternation T-maze test evaluating working memory. First, the NOR training was followed 24 hours later by a long-term memory test<sup>45</sup>. Both Piezo1<sup>cx/cx</sup>; *Cdh5*-Cre+ (GOF) and Piezo1<sup>cx/cx</sup>; *Slo1c1*-Cre+ (brain-EC-GOF) mice displayed significantly impaired long-term NOR memory compared with respective littermate controls, but no change in locomotor activity (Fig. 6a–f, Fig. S13). Second, we used the spontaneous alternation T-maze test to assess the natural tendency of mice to explore a novel arm over a familiar one, which induces them to alternate the choice of the goal arm across repeated trials<sup>46</sup>. The percentage of alternation, an index of working memory, was significantly lower in brain-EC-GOF mice compared with controls (Fig. 6g), consistent with impaired working memory. Furthermore, we observed choice latencies across consecutive trials in both groups, but the latency was stronger in Piezo1<sup>cx/cx</sup>; *Slo1c1*-Cre+ mice, consistent with poorer performance (Fig. 6h). As this is a newly developed brain EC Piezo1-GOF model, we characterized their general activity levels,

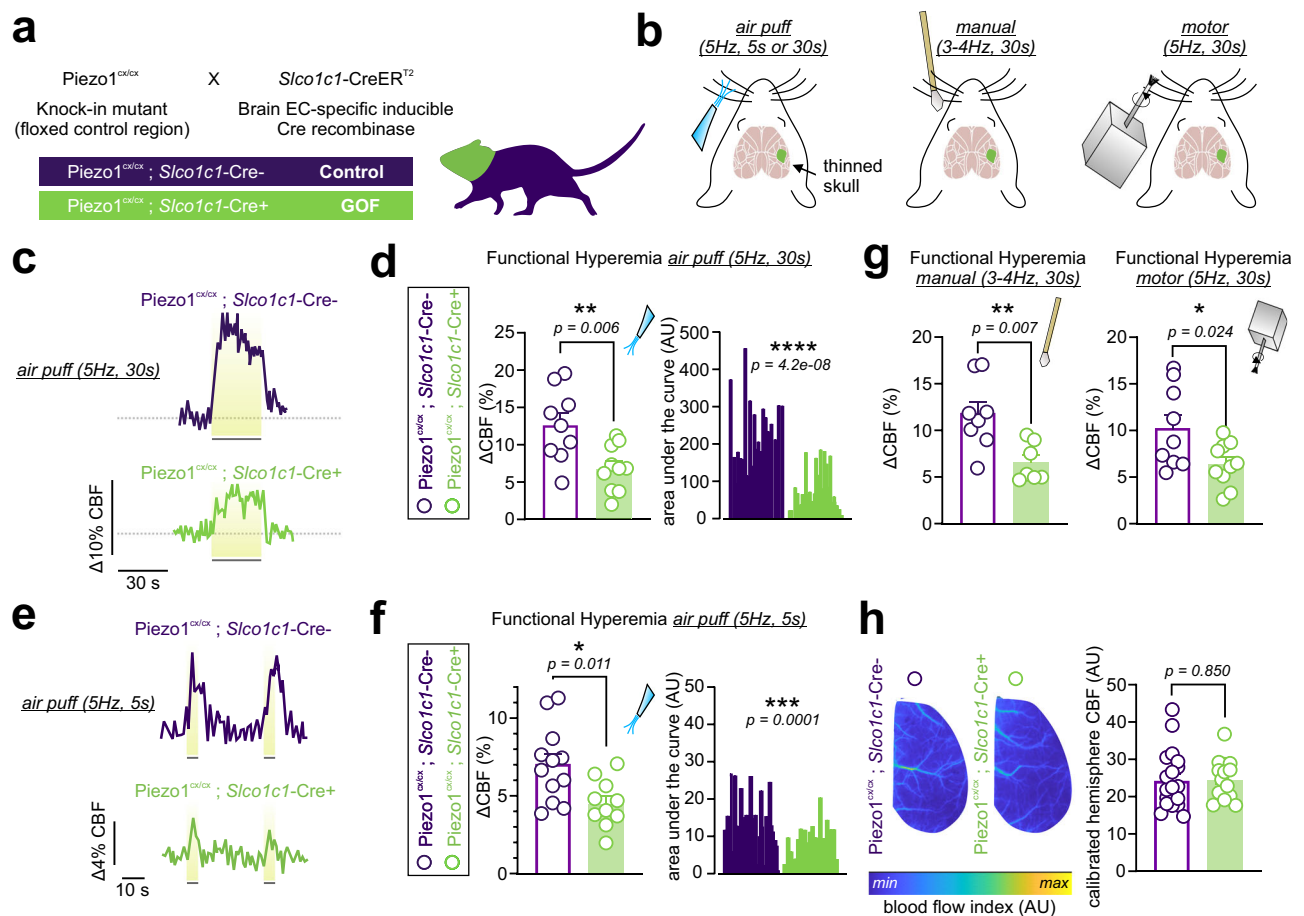


**Fig. 4 | Piezo1-GOF mutation in the brain vasculature impairs blood flow increase during somatosensory stimulation.** **a** Crossbreeding scheme used to generate inducible, brain EC-specific Piezo1-GOF (Piezo1<sup>lox/lox</sup>;Slco1c1-Cre<sup>+</sup>) mice. Tamoxifen-treated Cre<sup>+</sup> mice were used as GOF, and littermate Cre<sup>-</sup> mice were the control. **b** Schematic illustrations of different whisker stimulation paradigms during LSCI recordings (thinned skulls), with the contralateral somatosensory barrel cortex highlighted (green). **c** Representative traces of FH responses to air puffs (5 Hz, 30 s each) in a control and a Piezo1<sup>lox/lox</sup>;Slco1c1-Cre<sup>+</sup> mouse. **d** Scatter plot of CBF increases during 30 s air puff whisker stimulation in control ( $n = 9$ ) and brain EC-GOF ( $n = 10$ ) mice. *Right*: area under the curve analyses (control: 28 whisker stimulations; GOF: 32 stimulations). **e**, **f** Representative responses and summary data

of hyperemic responses to 5 s whisker stimulation using air puffs ( $n = 12$  control; 10 brain-EC-GOF). Area under the curve analyses compare 39 stimulations in brain-EC-GOF mice and 35 stimulations in controls. **g** Averaged scatter plots of FH responses to manual stimulation ( $n = 8$  control; 7 brain-EC-GOF) or motor stimulation ( $n = 9$  control; 10 brain-EC-GOF). **h** Examples and averages of baseline blood flow in the hemispheres of control ( $n = 19$ ) and brain-EC-GOF ( $n = 14$ ) mice. All statistical tests were unpaired Student's *t* test (two-sided, \* $P < 0.05$ , \*\* $P < 0.01$ , \*\*\* $P < 0.001$ , \*\*\*\* $P < 0.0001$ ). All error bars are SEM. Scatter plot data in **d**, **g**, **f**, **h** are presented as mean  $\pm$  SEM. Area under the curve data in **d** and **g** are presented as histograms. Source data are provided as a Source Data file.

motor coordination, and anxiety-like behavior. Both GOF strains had comparable physical activity (e.g., distance traveled, movement duration, motor coordination) and anxiety-like behavior (elevated plus maze and open field center time) with their respective controls (Figs. S14, S15). Slight alterations in motor coordination were observed in GOF and knockout mice, without impairment in motor learning and memory (rotarod; Fig. S16). These data collectively demonstrate that enhanced Piezo1 function in the brain endothelium, due to a human GOF mutation, is associated with memory impairment in mice.

## Discussion

Hyperemia in response to increased neuronal firing is important for sustaining brain health and function<sup>2,47</sup>. Several neurovascular coupling mechanisms have been identified whereby increased neural activity triggers the release of neurovascular coupling agents from neurons and astrocytes, which in turn act on the vasculature to cause hyperemia. Increased blood flow during FH sustains neural activity by delivering O<sub>2</sub> and nutrients and clearing metabolic waste<sup>1</sup>. Less is known, however, about feedback mechanisms underlying the recovery of blood flow to basal levels after hyperemia. Here, we fill this gap in

our understanding and provide functional evidence for a mechano-feedback system in which endothelial Piezo1 activation speeds up blood flow recovery to baseline at the conclusion of neural stimulation. This paradigm introduces Piezo1 as a sensor of hyperemia in the brain endothelium and highlights its role as a *built-in endothelial feedback system* with the potential to determine not only the magnitude but also the shape of the hyperemic response (Fig. S17).

Piezo1 is expressed throughout the vascular endothelium. Earlier investigations have identified that EC Piezo1 function is essential during embryonic vascular development<sup>48,49</sup>. Arterial Piezo1 activity during adulthood has been linked to the production of the potent vasodilator NO and to changes in endothelial V<sub>m</sub>, both of which had profound effects on vascular tone<sup>17,33</sup>. Our recent characterization of Piezo1 in the CNS vasculature showed that mechanical forces activate Piezo1, leading to inward cationic currents and Ca<sup>2+</sup> signals<sup>14</sup>. In the context of neurovascular coupling and CBF, different scenarios could be at play when brain EC Piezo1 channels are stimulated (Fig. S17). Localized Ca<sup>2+</sup> transients could activate endothelial NO synthase (eNOS) leading to the generation of the short-lived vasodilator NO, mural cell relaxation, and ultimately a local increase in blood flow<sup>50</sup>.

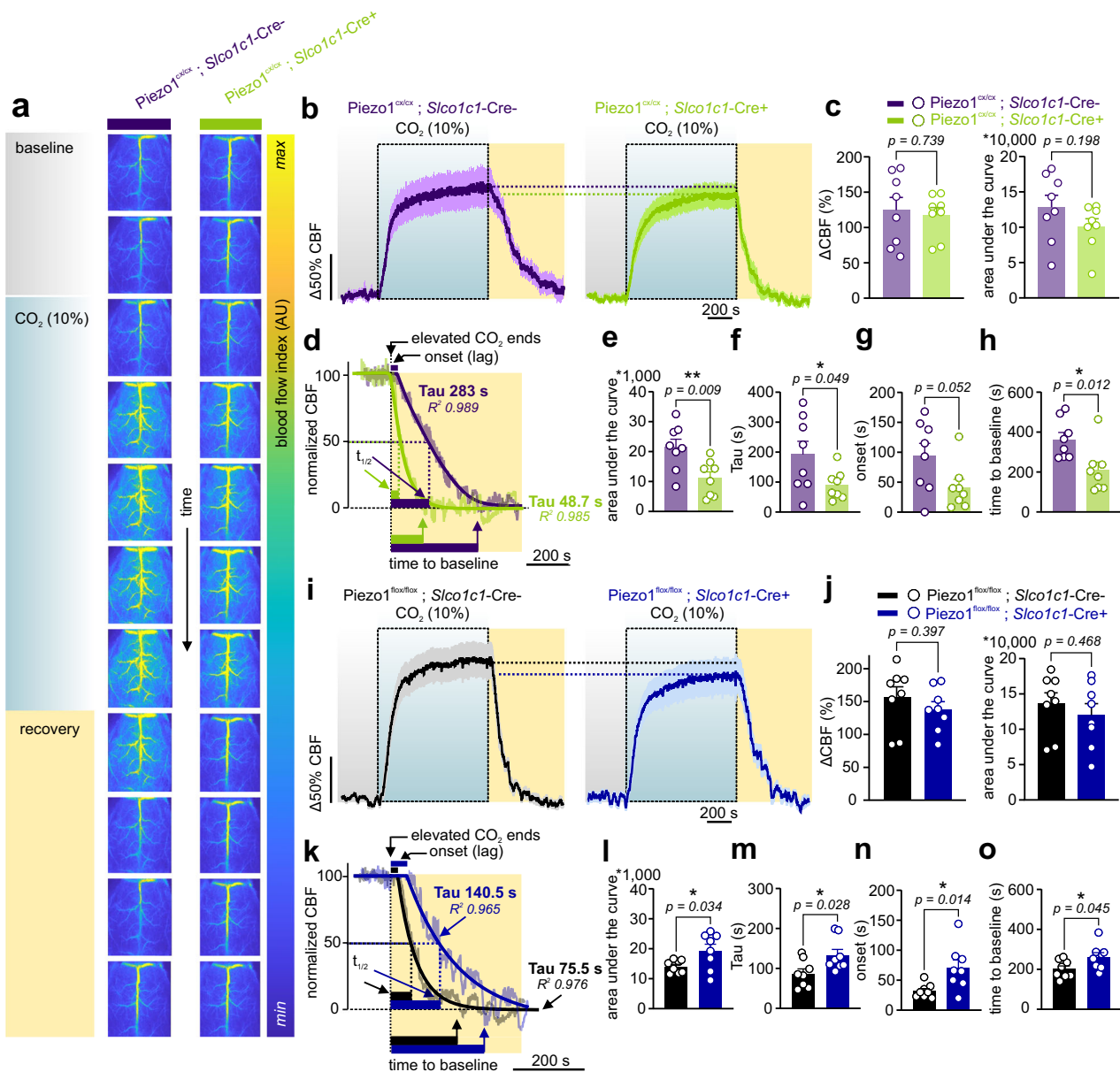


**Fig. 5 | CO<sub>2</sub>-induced hyperemia is altered in mice with enhanced or reduced brain EC Piezo1 activity.** **a** Representative consecutive images, recorded using LSCI through thinned skulls, reflect CBF responses to 10% CO<sub>2</sub> inhalation in a control (Piezo1<sup>lox/cx</sup>;Sico1c1-Cre<sup>-</sup>) and a Piezo1<sup>lox/cx</sup>;Sico1c1-Cre<sup>+</sup> mouse. A 5-min baseline was followed by 10% CO<sub>2</sub> (15 min), and then CBF was allowed to recover to baseline over 10 min. **b** Averaged normalized CBF changes in control and Piezo1<sup>lox/cx</sup>;Sico1c1-Cre<sup>+</sup> mice (n = 8 mice/group). **c** Maximal increases in CBF in response to hypercapnia and areas under the curve over the entire recording in control and brain-EC-GOF mice (n = 8 mice/group). **d** Representative CBF recovery in a control and a Piezo1<sup>lox/cx</sup>;Sico1c1-Cre<sup>+</sup> mouse. Plateau followed by exponential decline fittings of the recovery phase and the corresponding Tau and goodness of fit (R<sup>2</sup>). Additional kinetic parameters include recovery half-time (t<sub>1/2</sub>: time to 50% decrease), the duration required for return to baseline (time to baseline), and the

recovery onset (the lag between the end of CO<sub>2</sub> stimulation to the beginning of decline). **e** Area under the curve of 5-min of recovery in control and brain-EC-GOF mice (n = 8 mice/genotype). **f, g, h** Averaged scatter plots of kinetic parameters (Tau, onset, time to baseline), as shown in **d** (n = 8 mice/genotype). **i** Averaged normalized changes in CBF in control and Piezo1<sup>lox/lox</sup>;Sico1c1-Cre<sup>+</sup> mice. **j** Change in CBF in response to CO<sub>2</sub> in brain-EC-knockout mice and controls (n = 8 mice/group). **k** Representative traces and fittings of CBF recovery in a control and a Piezo1<sup>lox/lox</sup>;Sico1c1-Cre<sup>+</sup> mouse. **(l, m, n, o)** Area under the curve of 5-min of recovery and other kinetic parameters of the recovery phase in control and Piezo1<sup>lox/lox</sup>;Sico1c1-Cre<sup>+</sup> mice (n = 8 each). Data in **b, c, e–h, i, j, l–o** are presented as mean ± SEM. All statistical tests were unpaired Student's t test (two-sided, \*P < 0.05, \*\*P < 0.01), and all error bars are SEM. Source data are provided as a Source Data file.

Endothelial Ca<sup>2+</sup> signals could activate Ca<sup>2+</sup>-activated K<sup>+</sup> (K<sub>Ca</sub>) channels in arteries, leading to EC hyperpolarization that propagates to SMCs and triggers vasodilation<sup>51,52</sup>. However, most brain ECs (~80%) are capillary ECs<sup>53</sup>, where functional expression of K<sub>Ca</sub> channels is lacking<sup>8</sup>. Alternatively, Piezo1 could affect vascular tone and blood flow through EC depolarization due to cation influx, as has been shown before in peripheral arterial ECs<sup>17,18</sup>. The evidence presented here demonstrates that Piezo1 activation depolarizes ECs, consistent with a role for Piezo1

as a feedback mechanism to reset endothelial V<sub>m</sub>. We suggest that increases in Piezo1 inward depolarizing current during FH may surpass hyperpolarization and act as a short-circuit to reset V<sub>m</sub>. To reconcile our current observations with previous reports of localized Ca<sup>2+</sup> transients in proximal brain capillaries leading to NO-mediated increases in capillary red blood cell flux<sup>30</sup>, we speculate that the large-scale changes in hemodynamic forces—that occur during FH in tens of thousands of vascular segments—recruit many Piezo1 channels to cause strong



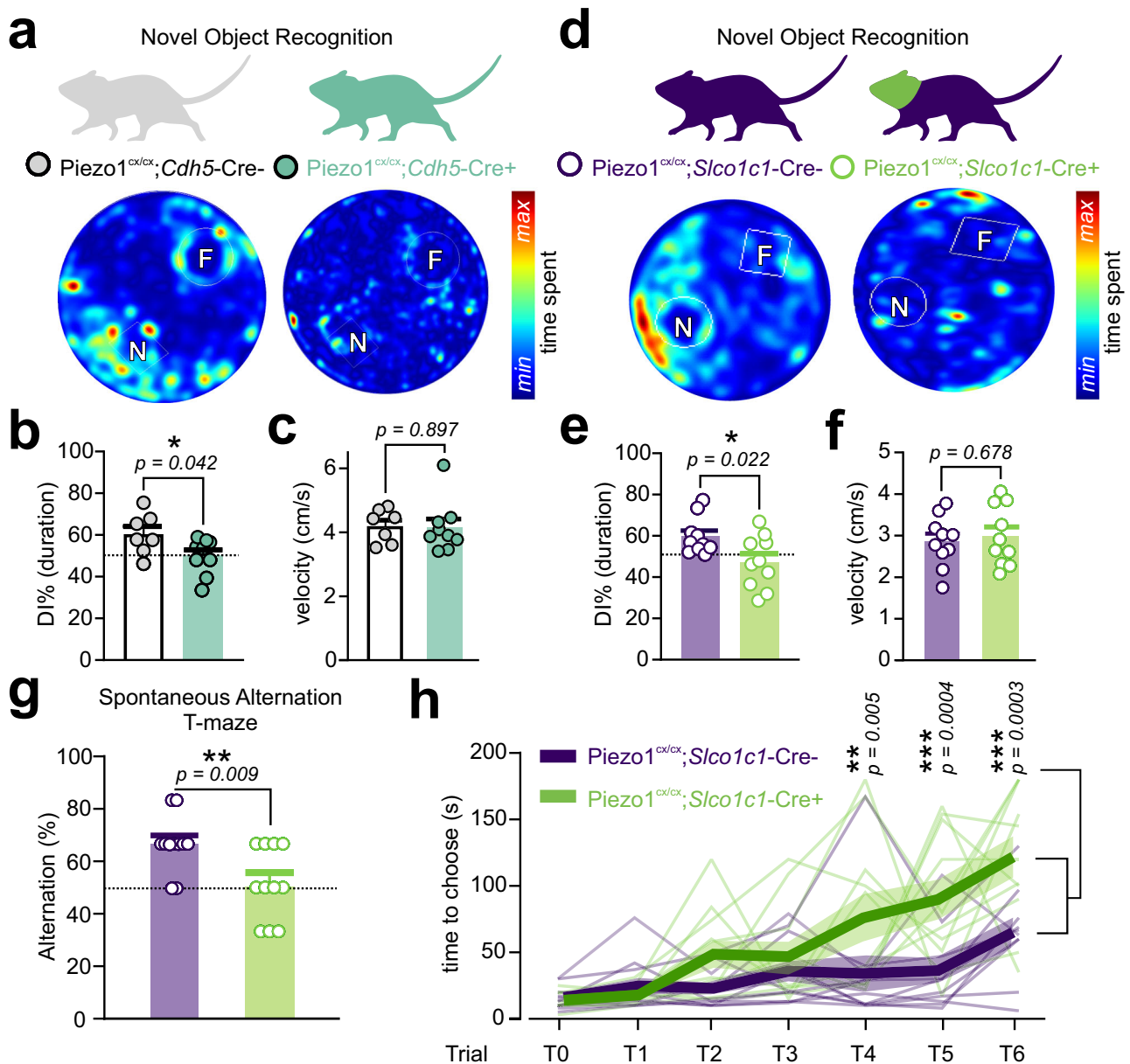


**Fig. 6 | Endothelial Piezo1 gain-of-function mice display a memory impairment phenotype.** **a** Novel object recognition test in control and Piezo1<sup>cx/cx</sup>;Cdh5-Cre<sup>+</sup> mice. Heat maps demonstrate the cumulative time spent with familiar (F) and novel (N) objects. **b** Scatter plot shows the discrimination index (DI%-calculated based on duration) for the two groups ( $n = 7$  control, 9 Piezo1<sup>cx/cx</sup>;Cdh5-Cre<sup>+</sup> mice). DI of 50% (dotted) indicates equal time spent with novel and familiar objects. **c** Velocities of control ( $n = 7$ ) and Piezo1<sup>cx/cx</sup>;Cdh5-Cre<sup>+</sup> mice ( $n = 9$ ) during the NOR test. **d, e** Similar to **a** and **b**, test results from Piezo1<sup>cx/cx</sup>;Slco1c1-Cre<sup>+</sup> and their controls ( $n = 10$  each). **f** Motor activity of Piezo1<sup>cx/cx</sup>;Slco1c1-Cre<sup>+</sup> mice and their controls ( $n = 10$  each) during the NOR test. **g** Percent of alternation over all 6 trials during the

spontaneous alternation T-maze was calculated as [(number of correct alternations/6)\*100] in Piezo1<sup>cx/cx</sup>;Slco1c1-Cre<sup>+</sup> and their controls ( $n = 11$  each). The dotted line represents the 50% chance level. **h** Choice latency in Piezo1<sup>cx/cx</sup>;Slco1c1-Cre<sup>+</sup> and control mice over trials 1 to 6. Asterisks highlight significantly higher choice latency in Piezo1<sup>cx/cx</sup>;Slco1c1-Cre<sup>+</sup> mice at T4, T5 and T6. Data from individual mice are shown, and bold lines and transparent shades are means and SEM, respectively ( $n = 11$  mice each). Statistical tests were unpaired Student's *t* test (two-sided, **b, c, e, f, g**) and two-way ANOVA test in **h** ( $*P < 0.05$ ,  $**P < 0.01$ ,  $***P < 0.001$ ). All error bars are SEM. Data in **b, c, e-g** are presented as mean  $\pm$  SEM. Source data are provided as a Source Data file.

depolarization (Fig. S17). Spatially restricted Piezo1-mediated depolarization to a small mechanical stimulus in a single capillary is likely too small and the electronic nature of depolarizing currents in ECs means they do not spread far enough to affect mural cells<sup>8,50</sup>. Importantly, we only observed endothelial Ca<sup>2+</sup>/NO-induced CBF increases in proximal capillaries that are covered with contractile pericytes—in contrast to deep capillaries where there was no correlation between Ca<sup>2+</sup> signals and blood flow<sup>50</sup>.

Functional hyperemia manifests as a rapid increase in CBF that quickly returns to baseline at the cessation of a brief neural

stimulation. Extended neural firing, on the other hand, leads to CBF increases that reach or approach a plateau<sup>2,47</sup>. Pathways mediating the increase in CBF have been extensively explored, but little is known about how CBF returns to baseline when neuronal firing ceases. Here, we provide strong evidence to support the conclusion that endothelial Piezo1 acts as a mechano-feedback mechanism. First, pharmacological or genetic enhancement of Piezo1 activity suppressed the magnitude of hyperemia in response to somatosensory stimulation. Second, EC Piezo1 deletion enhanced FH magnitude. Third, the kinetics of the hyperemic response were consistent with Piezo1 serving a feedback

role; Piezo1 activation slowed CBF increases, and accelerated blood flow return to baseline when stimulation terminated. Last, recovery of CBF to baseline after a non-somatosensory stimulation (i.e., hypercapnia) was evidently faster in mice with enhanced Piezo1 activity. Collectively, these lines of evidence support a fundamental role for EC Piezo1 as a mechano-feedback mechanism. While our data show that endothelial Piezo1 is an important factor for CBF recovery after hyperemia, Piezo1 deletion did not completely abolish hyperemia termination in Piezo1 knockout mice, suggesting that the mechano-feedback function described here is one of the main, but not the only, mechanism underlying active termination of hyperemia. Other mechanisms might involve astrocyte-derived factors, such as the vasoconstrictor 20-hydroxyeicosatetraenoic acid, or adenosine that could trigger neuronal inhibition<sup>13,54–57</sup>.

The endothelium plays an essential role in vascular function in general and in neurovascular coupling in particular<sup>38</sup>. Mechanosensing by vascular ECs is indispensable for vascular development, diameter and blood flow regulation. ECs are most affected by frictional forces due to blood flow, known as shear stress<sup>59</sup>. While shear has been classically linked to flow-mediated, endothelium-dependent vasodilation in the periphery<sup>60</sup>, flow constricts cerebral arteries and arterioles in a shear stress-dependent manner<sup>56,61,62</sup>. Flow-mediated vasoconstriction in the brain serves a protective role against general vasodilation, which would substantially increase CBF, blood volume, and intracranial pressure in a closed cranium. The latter effects would compress the brain parenchyma and could therefore be detrimental to brain function<sup>63</sup>. It should be noted that discrepant cerebrovascular responses to flow have been reported and attributed to factors such as intravascular pressure<sup>64–66</sup>. The evidence presented here—increased flow during FH leading ultimately to CBF reduction—is consistent with the centuries-old Monro-Kellie doctrine positing that the sum of volumes of intracranial blood, brain tissues, and cerebrospinal fluid remains constant with no net change<sup>67</sup>. Our data suggest that Piezo1-mediated sensing of FH-associated shear depolarizes ECs, short-circuits endothelial hyperpolarization mediated hyperemia/vasodilation<sup>8</sup>, and as such acts as a mechano-feedback system<sup>50–52</sup>.

While Piezo1 enhancement affected FH, there was no overt impact on baseline CBF. This could reflect insufficient forces (i.e., transient oscillatory hemodynamics) to trigger a mechano-feedback mechanism under baseline conditions. It could also be attributed to the extent of Piezo1 engagement (minutes after Yoda1, or days/weeks after induction in GOF mice) being sufficient to cripple FH, but not strong and sustained enough to alter baseline CBF. These possibilities await future investigations. FH occurs throughout the vascular tree in the somatosensory cortex (Fig. S17)—where Piezo1 is expressed in arteriolar, capillary and venular ECs<sup>14,22</sup>—and we speculate that entire vascular networks are implicated in the feedback mechanism. It remains unclear where within these networks the feedback mechanism predominates. Given that the majority of Ca<sup>2+</sup> transients in deep capillaries do not translate into vasodilation<sup>50</sup> and that capillary Ca<sup>2+</sup> signals do not trigger K<sub>Ca</sub>-mediated hyperpolarization<sup>8</sup>, we expect that capillaries are a major contributor to mechano-feedback mechanisms. Experimental investigations are required to determine the contribution of capillaries and arterioles to Piezo1-mediated braking.

FH has been canonically viewed as a mechanism that supplies the metabolic needs of active neurons. Alternative proposed functions for neurovascular coupling include cerebrovascular structure stabilization, temperature homeostasis, neurotransmitter synthesis, and cerebrospinal fluid circulation<sup>3,4,68,69</sup>. The influence of mechanical forces on these functions is an active research area, with recent evidence suggesting that Piezo1 is involved in cerebrospinal fluid flow regulation<sup>70</sup>. FH could also decrease capillary stalling by increasing pressure and breaking blood cell adhesion to enhance CBF<sup>5</sup>. Capillary un-stalling and cerebrospinal fluid circulation are examples of phenomena of

mechanical force alterations that could influence ECs<sup>5</sup>. Intriguingly, the impact of hyperemia in the brain extends beyond the endothelium. For instance, changes in vascular diameter could signal to neurons, through vasculo-neuronal coupling, and alter astrocyte activity and interneuron spiking<sup>56,71</sup>. Sensing the forces associated with brain parenchyma deformation could be attributed to molecular players expressed in neurons, astrocytes, and microglia<sup>24,72–74</sup>. Collectively, hemodynamic changes associated with hyperemia could affect mechanosensory signaling through different mechanisms and cell types.

This study provides evidence that abnormal endothelial Piezo1 function is associated with altered learning and memory. Specifically, Piezo1 gain-of-function impairs FH and is associated with deficits in learning and recognition memory and working memory. Memory deficits were not explained by underlying changes in locomotor activity, motor learning or anxiety-like behavior, suggesting that the impact of Piezo1 in ECs could be selective for more subtle alterations in cognition. While our genetic manipulations impact the entire brain vasculature, our observations suggest a role for EC Piezo1-mediated mechanosensory feedback in the prefrontal-hippocampal network given their role in the recognition and working memory tasks we utilize here<sup>75–77</sup>. Recent studies suggest that neurovascular coupling and EC function differ between the hippocampus and neocortex<sup>78</sup>, providing avenues for future studies to dissect the role of brain-region specific Piezo1 in CBF regulation and cognition. Whether the neurovascular impairment is responsible for cognitive deficits in GOF mice remains to be confirmed. Together, our observations add to a growing literature implicating a critical role of Piezo1 in mediating mechanosensory feedback across different cell types that underlie cognition, including astrocytes<sup>23</sup>, microglia<sup>24</sup>, neurons<sup>73</sup>, and now vascular ECs.

Mechanosensing involves a force and a sensor. When hemodynamics (i.e., force), endothelial Piezo1 (i.e., sensor), or both are altered, disrupted mechano-sensation and -transduction ensue, leading to endothelial dysfunction. Hemodynamic disruptions and blood flow deficits are hallmarks of vascular diseases such as hypertension and atherosclerosis<sup>79,80</sup>. Chronic changes in neurovascular coupling could manifest as impaired vasodilation, blood flow alterations, and delayed responses, all of which represent hemodynamic alterations that adversely affect brain health. We anticipate that re-envisioning cerebrovascular disease through the defective-mechanosensing lens will be an area for future research. An important implication for this work relates to the growing number of human *PIEZO1* mutations<sup>26,81,82</sup>. The gain-of-function mice used here carry a *PIEZO1* mutation that in humans causes hereditary xerocytosis<sup>25,26</sup>, and other *PIEZO1* GOF mutations are prevalent in people of African descent<sup>25,83,84</sup>. Loss of function *PIEZO1* mutations have also been reported and linked to disorders such as lymphatic dysplasia<sup>82</sup>. Since there is clear evidence that FH has an important physiological role, and the evidence presented here demonstrates that Piezo1 dictates the magnitude and shape of hyperemia, it will be important to explore whether human *PIEZO1* mutations adversely impact brain function and could therefore be risk factors for dementia.

In summary, this study provides evidence that endothelial Piezo1 channels serve a mechano-feedback role in CBF control. This introduces the mechanical hemodynamic forces not only as a result and an endpoint of hyperemia, but also as a trigger to engage Piezo1-mediated mechanosensation as a major regulator of brain blood flow.

## Methods

All experimental protocols used in this study are in accord with institutional guidelines and approved by the Institutional Animal Care and Use Committee (IACUC) of the University of Vermont (protocol X1-063) and the University of Maryland (protocol 1121009). This study complies with ARRIVE guidelines.

## Animal models

Adult (3–5-month-old) male and female mice were group-housed on a 12-hour light: dark cycle with environmental enrichment and free access to food and water. Mice used include wild-type C57BL/6J mice (Jackson Laboratories, USA). Inducible, EC-specific Piezo1-knockout ( $Piezo1^{fl/fl}; Cdh5-Cre+$ ) mice were generated by crossing mice in which exons 20–23 of the *Piezo1* gene are flanked by loxP sites ( $Piezo1^{fl/fl}$ ; Jackson Laboratories, JAX stock 029213) with mice expressing an inducible *Cre*-recombinase under the transcriptional control of *Cdh5* ( $Cdh5-CreER^{T2}$ ). Tamoxifen-inducible, Piezo1 gain-of-function ( $Piezo1^{cx/cx}; Cdh5-Cre+$ ) mice were engineered by crossing  $Cdh5-CreER^{T2}$  and knock-in  $Piezo1^{cx/cx}$  mice (Taconic Biosciences, Model No. 21617) in which floxed exons 45–51 are followed by a mutant Piezo1 copy (R2482H mouse mutation- equivalent to R2456H in humans)<sup>25,85</sup>. Homozygous mice were used as GOF (*Cre+*) or controls (*Cre-*). Inducible, brain-EC-specific Piezo1-GOF ( $Piezo1^{cx/cx}; Slco1c1-Cre+$ ) or knock-out ( $Piezo1^{fl/fl}; Slco1c1-Cre+$ ) mice were engineered by crossing the transgenic *Slco1c1-CreER<sup>T2</sup>* strain<sup>34,35</sup> with knock-in  $Piezo1^{cx/cx}$  or floxed  $Piezo1^{fl/fl}$  mice.  $Piezo1^{fl/fl}$  mice were originally generated in C57BL/6J background and  $Piezo1^{cx/cx}$  mice were initially generated in BALB/c background. *Cdh5-Cre* and *Slco1c1-Cre* mice were in the C57BL/6 background. For induction of *CreER<sup>T2</sup>*, offspring homozygous for floxed *Piezo1* ( $Piezo1^{fl/fl}$ ) or knock-in  $Piezo1^{cx/cx}$  and expressing *Cre*-recombinase were treated with tamoxifen by providing tamoxifen citrate food (Envigo, TD.130859) for 7 consecutive days (daily tamoxifen intake, ~40 mg/kg). Tamoxifen treatment was followed by a washout period before experimental intervention (3–5 weeks for CBF experiments, 7–10 weeks for behavioral studies). Tamoxifen-treated littermates of similar backgrounds that lacked *Cre*-recombinase expression (*Cre-*) were used as controls. A cohort of mice received no tamoxifen and were used to study potential impact of genetic backgrounds, independent of Piezo1 manipulation. Animals were euthanized by intraperitoneal injection of sodium pentobarbital (100 mg/kg) or by isoflurane inhalation followed by rapid decapitation. Animals of both sexes were used; animal assignments to experimental groups sex were randomized so that approximately equal number of male and female mice were incorporated per group.

## Laser Doppler flowmetry

After anesthetizing mice with isoflurane (5% induction, 2% maintenance, Somnoflo, Kent Scientific), a catheter was inserted into the femoral artery and connected to a pressure transducer to monitor blood pressure. All laser Doppler flowmetry experiments utilized acute cranial window over the somatosensory cortex, and the dura mater was removed. The window was superfused with aerated, warm (37 °C) artificial cerebrospinal fluid throughout the experiment to ensure that cortex temperature was maintained. Functional hyperemia was induced by whisker stimulation and measured in the mouse somatosensory cortex<sup>9</sup>. Cortical CBF was recorded through the cranial window with a laser Doppler probe (PeriMed) under the combined anesthesia of  $\alpha$ -chloralose (50 mg/kg) and urethane (750 mg/kg). Functional hyperemic responses are presented as the percent change in CBF induced by stroking the contralateral vibrissae at a frequency of ~3–4 Hz for 60s (i.e., whisker stimulation) relative to the baseline value. We and others have previously shown that 60s long whisker stimulation is sufficient to accurately capture differences in hyperemia amplitude and kinetics after the application of pharmacological agents or in genetically modified mice<sup>9,86,87</sup>. In some experiments, Yoda1 was topically applied by adding to the cortical superfusate. We have previously shown that cortical application of drugs and pharmacological modulators can alter cerebral endothelial signaling<sup>8,9</sup>. Intravenous administration of Yoda1 was avoided because RBCs express functional Piezo1 channels and can therefore change shape in response to Yoda1<sup>25</sup>. Intraperitoneal injection was not employed, since there is no evidence that Yoda1 can reach the cerebrovasculature through this

route. During CBF measurements, blood pressure was continuously recorded via the femoral artery cannula, and body temperature was maintained at 37 °C using a servo-controlled heating pad with a rectal temperature sensor probe. All data were recorded and analyzed using LabChart 8 software (AD Instruments).

## Two-photon laser-scanning microscopy (2PLSM)

Mice were anesthetized with inhaled isoflurane (3% induction, 1.5% maintenance). Thermal support was provided using a feedback-controlled heating pad (Harvard Apparatus). FITC-dextran (2000 kDa, 150  $\mu$ L, 1 mg/ml) was injected retro-orbitally to visualize the vasculature. The skull was exposed and a titanium headplate was affixed. The mouse was then mounted to a frame for imaging on a Scientifica Hyperscope (Scientifica, UK) coupled to a Coherent Chameleon Vision II Titanium-Sapphire pulsed fs laser (Coherent, USA) equipped with an Olympus 20x infinity-corrected Plan Fluorite 1.0 NA water-immersion objective. A cranial window (approximately 2 mm diameter) was drilled into the skull and the dura was removed. Upon completion of the surgery, isoflurane anesthesia was replaced with  $\alpha$ -chloralose (50 mg/kg) and urethane (750 mg/kg). Penetrating arterioles (PA) were identified by morphology and directionality of RBC flow. Artificial cerebrospinal fluid aerated with 20% O<sub>2</sub>/5% CO<sub>2</sub> was maintained at 37 °C and superfused over the cranial window at a rate of ~1 mL/min and monitored with a temperature probe throughout the duration of the experiment. Drugs were dissolved in the circulating aCSF and were superfused for 20 minutes prior to imaging. Penetrating arterioles were visualized for a baseline period prior to stimulus. The whisker stimulus consisted of a series of air puffs at 20 PSI at a rate of 5 Hz (10 ms on/190 ms off) delivered to the contralateral whiskers of the animal. Diameter measurements across time were measured using a custom MATLAB script written by D. Isaacs that calculated the full width at half maximum (FWHM) of a line profile placed over a PA for each frame of the xyt recording. To avoid contamination by shot noise and other sources, once the FWHM of the line profile for the PA under study had been calculated for each frame, any individual value greater than 3\*SD (standard deviation) from the baseline mean was replaced with NaN in the diameter vs. time trace. Where possible, multiple trials were performed and averaged in each mouse. The baseline was defined as the average FWHM in  $\mu$ m in the 25 s prior to stimulation and this served as the reference point in the percent change in diameter measurements. The change in diameter extracted from the data describes the maximal change observed relative to the baseline established for the PA being imaged.

## Laser Speckle Contrast Imaging (LSCI)

Mice were first anesthetized by inhalation of 4–5% isoflurane for induction and then 2% for maintenance, followed by intraperitoneal injection of  $\alpha$ -chloralose (50 mg/kg) and urethane (750 mg/kg). To prevent excess lung secretions during experiments, mice were given atropine (0.05 mg/kg, subcutaneous). For the duration of the procedure and imaging, we used a thermometer and feedback-controlled heating blanket (RWD) to maintain body temperature at 37 °C. Mice were shaved and positioned in a stereotaxic frame to immobilize the head. The surface tissue overlying the cranium was removed surgically, the skull was exposed, thinned using a microdrill or a scalpel and covered with agarose and a glass coverslip (thickness size 0). A custom-built laser speckle contrast imaging (LSCI) setup was used for imaging blood flow dynamics in real-time through the thinned skull, as described before<sup>88,89</sup>. The LSCI setup included delivering coherent near-infrared (NIR) light using a laser diode (785 nm, LP785-SAV50, Thorlabs) controlled using a diode driver (CLD1010LP, Thorlabs). Backscattered light was recorded using a zoom imaging lens (VZM 450i, Edmund Optics) mounted on an NIR-sensitive CMOS camera (Basler ace acA2000-165um NIR, Basler, Germany). LSCI data were analyzed by calculating an arbitrary blood flow index which represents

$1/K^2$  where  $K$  is contrast. While LSCI is generally used to measure relative changes in blood flow, we measured absolute blood flow index while parameters were held constant so that we could make comparisons of calibrated baseline hemisphere blood flow<sup>90</sup>. Baseline and stimulation recordings were made over a field of view 8x8mm with 1024x1024 pixels with a frame rate of 50 Hz (50 frames per second [fps]) or 15 fps for hypercapnia experiments. Data were acquired using custom-built acquisition software and processed using spatial speckle contrast analysis to get a high temporal resolution. Customized MATLAB scripts were used to process and analyze LSCI data. Differential hyperemia mapping was routinely used to locate the region with maximal response during whisker stimulation (i.e., barrel cortex). Recordings were made at lower (0.75X) and higher (2X) magnifications to reveal the whole contralateral hemisphere or the somatosensory cortex, respectively. Whiskers were stimulated during LSCI using air puffs (AIRSTIM, San Diego Instruments or custom-built air stimulator) for 5 or 30 s at 5 Hz. Motor stimulation was achieved using a custom-built device (5 Hz), and manual stimulation was achieved by stroking the contralateral vibrissae at 3-4 Hz. Hypercapnia was induced by mixing the inspired oxygen-enriched air with 10% CO<sub>2</sub> using a flowmeter (MF5700, ATO).

To achieve reliable and repeatable measurements with LSCI, we ensured that the imaging parameters were in optimal range – the speckle-to-pixel size ratio was maintained at approximately 2<sup>91</sup>, a stabilized laser diode with long coherence length was used<sup>92</sup>, and a linear polarizer in cross-polarization configuration was installed<sup>90,93</sup>. The parameters were maintained constant, and no changes to the system were introduced during the study. Furthermore, we have validated the parameters' stability by measuring the contrast of static scattering phantom several times during the study and found it unchanging. These steps ensure that LSCI measurements are compatible longitudinally and between the animal groups. Furthermore, in the analysis step, we minimized the possible influence of the skull tissue on the BFI measurements by using temporal contrast analysis over 25 consecutive frames, which is known to be less sensitive to static scattering<sup>94</sup>.

### Endothelial cell isolation

Single capillary ECs were obtained from mouse brains by mechanical disruption of ~10–15 mm<sup>3</sup> of somatosensory cortical tissue using a Dounce homogenizer<sup>14</sup>. Tissues were homogenized in ice-cold isolation buffer (124 mM NaCl, 3 mM KCl, 2 mM CaCl<sub>2</sub>, 2 mM MgCl<sub>2</sub>, 1.25 mM NaH<sub>2</sub>PO<sub>4</sub>, 26 mM NaHCO<sub>3</sub>, 4 mM glucose), and homogenates were passed through a 62- $\mu$ m nylon mesh. The filtered vasculature retained on the nylon mesh was eluted using a dissociation solution (55 mM NaCl, 80 mM Na-glutamate, 5.6 mM KCl, 2 mM MgCl<sub>2</sub>, 4 mM glucose, 10 mM HEPES pH 7.3) containing protease (0.5 mg/mL), elastase (0.5 mg/mL; Worthington, USA) and 100  $\mu$ M CaCl<sub>2</sub>, and the suspension was incubated for 23 min at 37 °C. After adding 0.5 mg/mL collagenase Type I (Worthington, USA) and incubating for 2 min, the suspension was filtered, and the enzymes were removed by washing the retained material with isolation buffer. Single ECs were dispersed by triturating -3-5 times using a glass Pasteur pipette. A few drops of the EC suspension were added to the recording chamber containing enzyme-free dissociation solution. Cells were used within ~6 hours of dispersion.

### Patch clamp electrophysiology

Piezo1 single-channel currents were recorded<sup>14</sup> in the cell-attached configuration using an Axopatch 200B patch-clamp amplifier (Molecular Devices). Recordings were filtered at 1 kHz, digitized at 5 kHz, and stored for subsequent analysis with Clampfit 10.3 software. We used a sampling rate of 20 kHz, and a low-pass filter frequency of 1 kHz. The bath solution was composed of 140 mM KCl, 1 mM MgCl<sub>2</sub>, 10 mM HEPES, 4 mM glucose, and 2 mM CaCl<sub>2</sub> (pH 7.35). Using a Narishige

puller, recording pipettes were pulled from borosilicate glass (1.5 mm outer diameter, 1.17 mm inner diameter; Sutter Instruments, USA). Pipette tips were fire-polished using a Narishige microforge to reach a tip resistance of ~4 M $\Omega$ . The pipette solution was composed of 3 mM KCl, 137 mM NaCl, 1 mM MgCl<sub>2</sub>, 10 mM HEPES, 4 mM glucose, and 2 mM CaCl<sub>2</sub> (pH 7.35). In some experiments, the pipette solution was supplemented with Yoda1. Representative current traces presented depict the median for each genotype or experimental condition. The minimum recording duration from an EC was 300s.

### Sharp electrode recordings

Membrane potential ( $V_m$ ) was measured using sharp microelectrode impalements of capillary ECs freshly isolated from *Pdgfrb-Cre-TdTomato* mice. Cortical tissue from one brain hemisphere was extracted in an isolation buffer and minced into smaller pieces with microscalpels as described before<sup>95</sup>. Minced tissue was incubated with enzyme P (Neural Tissue Dissociation kit, Miltenyi Biotec, USA) for 18 min at 37 °C, followed by the addition of enzyme A, homogenization by passing through a 21 G needle -4 times and incubation for 15 min at 37 °C. The homogenate was again passed through the 21 G needle -5 times and incubated for 12 min at 37 °C, and the resulting cell suspension was filtered through a 62- $\mu$ m nylon mesh and stored in ice-cold isolation buffer solution. Cells were allowed to adhere to a perfusion chamber coated with a silicone elastomer (SYLGARD 182), and TdTomato-negative ECs on capillaries were identified for impalement using fluorescence and brightfield microscopy. The chamber was perfused with bath solution (137 mM NaCl, 3 mM KCl, 2 mM CaCl<sub>2</sub>, 4 mM glucose, 1 mM MgCl<sub>2</sub>, and 10 mM HEPES, pH 7.4), and cells were impaled using sharp microelectrodes filled with 0.5 M KCl (resistance > 100 M $\Omega$ ). AxoClamp 900A digital amplifier and HS-2 headstage (Molecular Devices, USA) were used for recording  $V_m$ , and Axon Digidata 1550B and pClamp 9 software were used for signal digitization and analyses.  $V_m$  was measured at baseline and in the presence of Yoda1. Only recordings with a stable baseline prior to impalement, sharp negative deflection of  $V_m$  upon impalement, and return to 0 mV on withdrawing the electrode were considered for analysis.

### Immuno-histological staining

Staining was performed in free-floating vibratome sections as described before<sup>27</sup>. Briefly, brain tissue was postfixed in 4% paraformaldehyde for 4-6 hours before being stored in PBS with 0.02% Na-azide. Using a vibratome (Leica VT1200S), 50  $\mu$ m thick coronal tissue sections were prepared. Before the staining of brain sections, pepsin antigen retrieval was performed for 5 min at 37 °C (0.01 mg/ml pepsin in PBS, 0.2N HCl) for the staining of the vasculature and string vessels. Sodium citrate buffer (10 mM, pH 6.0, 95 °C for 10 min) based antigen retrieval was performed for the staining of pericytes. All other stains did not need antigen retrieval procedures. For blocking, we used 3% BSA in PBS containing 0.3% Triton X-100 for 6h at room temperature. Incubation with primary antibodies was performed at 4 °C for 48h, while incubation with secondary antibodies was performed in blocking solution at 4 °C overnight. Endothelial cells were stained using an anti-caveolin 1 antibody (Cell Signaling Technology, #3267, 1:400, RRID: AB\_2275453) or an anti-CD31 antibody (Bio-Rad, #MCA2388, 1:200, RRID: AB\_2161026), basement membrane was stained using an anti-collagen IV antibody (Bio-Rad, #134001, 1:200, RRID: AB\_2082646), an astrocytic subpopulation was stained using an anti-GFAP antibody (Millipore, #AB5541, 1:200, RRID: AB\_177521), microglia were stained using an anti-Iba1 antibody (Abcam, #ab5076, 1:400, RRID: 2224402), neurons were stained using an anti-NeuN antibody (Millipore, #MAB377, 1:500, RRID: AB\_2298772) or a neurofilament 200 (NF200) antibody (Abcam, #ab8135, 1:1,000, RRID: AB\_306298), pericytes were stained using a PDGFR $\beta$  antibody (Cell Signaling Technology, #3169, 1:100, RRID: AB\_2162497), and an anti- $\alpha$ -SMA antibody was used to stain for contractile mural cells (Millipore, #C6198, 1:200, RRID:

AB\_476856). The following secondary antibodies were used (all diluted 1:400): anti-goat IgG coupled to Alexa Fluor 647 (Thermo Fisher Scientific, #A-21447, RRID: AB\_2535864); anti-rabbit IgG coupled to Alexa 488 (Thermo Fisher Scientific, #A-21206, RRID: AB\_2535792), anti-chicken IgG coupled to Cy3 (Jackson ImmunoResearch, #703-165-155, RRID: AB\_2340363), anti-mouse coupled to Alexa Fluor 488 (Life Technologies, #A-21202, RRID: AB\_141607), and anti-rat coupled to Alexa Fluor 647 (Abcam, #ab150155, RRID: AB\_2813835). Images were taken using confocal microscopes (Leica, SP5 and Stellaris 5). Image stacks were taken (50  $\mu\text{m}$  thickness, 5  $\mu\text{m}$  steps) and analyses were performed on z-projections. Empty basement membrane tubes (string vessels) were defined as endothelial-negative and basement membrane-positive structures, thinner than 4  $\mu\text{m}$  and measured manually using ImageJ. SMA-positive vessel length, PDGFR $\beta$ -negative vessel length, and diameter were measured manually using ImageJ. Vascular density, as well as the percentage of positive cell areas (GFAP, Iba1, NeuN) and mean intensity of neurofilament, were measured automatically using ImageJ<sup>27,96</sup>. The cortical and hippocampal regions were similar and consistent across the acquisition and between the samples. Cortical images contained layers 2-4 and hippocampal images were taken in the regions of the dentate gyrus and CA1. Imaging and analyses were performed in a blinded fashion.

### Behavioral studies

We used mice in which the Cre recombinase was induced with tamoxifen -7-10 weeks prior to cognitive assessment. Mice were individually handled for at least 7 days before starting behavioral studies. Additionally, mice were allowed a minimum of 1 h for acclimatization to the experimental room before training sessions or tests were performed. A sky-view camera system, suspended above the arena, was used in video recording in the absence of an examiner and the video was tracked and analyzed using EthoVision XT 16 software (Noldus Information Technology Inc., The Netherlands). Our behavioral battery was ordered as follows: open field, rotarod, and novel object recognition, to enable early testing of early anxiety and locomotor phenotypes unconfounded by later cognitive tests while enable additional habituation necessary for the more sensitive memory testing.

**Open field test.** Mice were individually placed in a circle-shaped arena and were allowed to move freely for 10 min. The arena was cleaned during intervals between different mice. The arena (46 cm diameter) was divided during analysis into a central zone (24 cm diameter) and a peripheral zone using EthoVision. The parameters analyzed were the total distance traveled, the number of entries to different zones, time spent in each zone, and the cumulative movement and non-movement time.

**Novel object recognition test.** Long-term memory was assessed using the novel object recognition (NOR) test. Mice were habituated for 6-8 days in a circular arena (30 cm diameter). A 10-min training phase followed habituation, where mice were introduced to two identical (familiar) objects. 24 h later, mice were subjected to a 5-min test phase. The test phase involved a novel object replacing one of the familiar objects (NOR). The arena and objects were cleaned between tests for different mice. The time spent with and frequency of interacting with different objects were calculated using EthoVision. The Discrimination Index (DI) was calculated using the formula:

$$DI = [NO / (NO + FO)] * 100,$$

where NO is the time spent or the frequency (i.e., number of interactions) of exploring the novel object and FO is the time spent or the frequency of exploring the familiar object. DI% above 50% indicated discriminative behavior towards novelty.

**Spontaneous alternation T-maze test.** As shown previously<sup>46</sup>, we used a T-Shaped maze consisting of three arms (start arm and lateral goal arms), all of which were 35 cm long and 7 cm wide. The floor and lateral walls of the maze were made of polymethyl methacrylate, with the lateral walls transparent and 15 cm high (to prevent mouse falling). Each arm had a guillotine door (16 cm high, 7 cm wide, and 2 mm thick). The maze was placed in a quiet and dimly lit room, and the same maze was used for all trials. In the sample trial (T0), the mouse was placed in the distal end of the start arm and allowed to freely explore and make a choice within 180 s per trial. Once the mouse entered the goal arm with the four paws and the tail, the door was closed to confine the mouse in the chosen arm for 30 seconds. At the end of the confinement period, the mouse was removed gently and placed back to the distal end of the start arm. Trials T1 to T5 were performed with the same steps, and the last trial (T6) was performed without confinement. For each mouse, from T1 to T6, the rate at which they chose a different arm than that explored in the previous trial (correct alternation) was calculated as:

$$\text{Alternation \%} = (\text{total number of correct alternations} / 6) * 100.$$

Total number of correct alternations must range between 0 and 6, and therefore the calculated alternation percent had to be one of the following values: 0, 16.7, 33.3, 50, 66.7, or 83.3%. The choice latency (time to choose) was measured from the time the mouse was placed in the distal end of the start arm till the mouse entered the goal arm, whether correct or not.

**Elevated plus maze test.** The anxiety response was evaluated using the elevated plus maze test. The stainless-steel apparatus used had four arms (two open arms without walls and two enclosed arms). Each arm was 30 cm long and 5 cm wide, and was attached to sturdy metal legs at an elevation of 40 cm. The mouse was placed in the center of the plus maze facing the open arm, and the number of entries and the time spent in each arm were tracked and recorded over a 5 min test. The apparatus was cleaned and dried between mice.

**Rotarod test.** The neuromuscular coordination was assessed using the rotarod test. Mice were placed on a cylindrical rod rotating at increasing speed. Each trial was 5 min and the time needed for mice to fall off the rod (latency to fall) was assessed. The test was over two consecutive days, with 5 trials per day.

### Statistical analysis

Data in figures and text are presented as means  $\pm$  standard error of the mean. All experiments were performed in a randomized manner (animals, pharmacological treatments). Statistical tests included paired and unpaired Student's *t* test. Non-parametric tests were used as specified in figure legends (Mann Whitney test or Wilcoxon test) when datasets did not pass normality tests or when tests of normality were not powered to detect departures from normality (e.g., when *n* is small [ $\leq 6$ ]). Choice latency for the spontaneous alternation T-maze was analyzed using two-way ANOVA test. Rotarod analysis was performed with a mixed effects ANOVA where Genotype was the between subjects' measure and Time was the repeated measure; Geisser-Greenhouse correction was applied. Analysis of binned traveled distances in the open field test was performed with a mixed effects ANOVA where Genotype was the between subjects' measure and Time was the repeated measure; Geisser-Greenhouse correction was applied. Statistical tests were performed using GraphPad Prism 10 software. *P*-values < 0.05 were considered statistically significant.

### Reporting summary

Further information on research design is available in the Nature Portfolio Reporting Summary linked to this article.

## Data availability

Source data are provided with this paper. All other data are available upon request.

## References

1. Iadecola, C. The Neurovascular Unit Coming of Age: A Journey through Neurovascular Coupling in Health and Disease. *Neuron* **96**, 17–42 (2017).
2. Schaeffer, S. & Iadecola, C. Revisiting the neurovascular unit. *Nat. Neurosci.* **24**, 1198–1209 (2021).
3. Rasmussen, M. K., Mestre, H. & Nedergaard, M. Fluid transport in the brain. *Physiol. Rev.* **102**, 1025–1151 (2022).
4. Yablonskiy, D. A., Ackerman, J. J. H. & Raichle, M. E. Coupling between changes in human brain temperature and oxidative metabolism during prolonged visual stimulation. *Proc. Natl Acad. Sci. USA* **97**, 7603–7608 (2000).
5. Drew, P. J. Neurovascular coupling: motive unknown. *Trends Neurosci* **45**, 809–819 (2022).
6. Das, A., Murphy, K. & Drew, P. J. Rude mechanicals in brain haemodynamics: non-neural actors that influence blood flow. *Philosophi. Trans. Royal Soc. B* **376**, 20190635 (2021).
7. Bean, B. P. The action potential in mammalian central neurons. *Nat. Rev. Neurosci.* **8**, 451–465 (2007).
8. Longden, T. A. et al. Capillary K<sup>+</sup>-sensing initiates retrograde hyperpolarization to increase local cerebral blood flow. *Nat. Neurosci.* **20**, 717–726 (2017).
9. Dabertrand, F. et al. PIP<sub>2</sub> corrects cerebral blood flow deficits in small vessel disease by rescuing capillary Kir2.1 activity. *Proc Natl Acad Sci USA* **118**, e2025998118 (2021).
10. Sancho, M. et al. Adenosine signaling activates ATP-sensitive K<sup>+</sup> channels in endothelial cells and pericytes in CNS capillaries. *Sci Signal* **15**, eabl5405 (2022).
11. Lacroix, A. et al. COX-2-Derived Prostaglandin E2 Produced by Pyramidal Neurons Contributes to Neurovascular Coupling in the Rodent Cerebral Cortex. *J. Neurosci.* **35**, 11791–11810 (2015).
12. Hoiland, R. L. et al. Nitric oxide is fundamental to neurovascular coupling in humans. *J. Physiol.* **598**, 4927–4939 (2020).
13. Attwell, D. et al. Glial and neuronal control of brain blood flow. *Nature* **468**, 232–243 (2010).
14. Harraz, O. F., Klug, N. R., Senatore, A. J., Hill-Eubanks, D. C. & Nelson, M. T. Piezo1 Is a Mechanosensor Channel in Central Nervous System Capillaries. *Circ. Res* **130**, 1531–1546 (2022).
15. Coste, B. et al. Piezo1 and Piezo2 Are Essential Components of Distinct Mechanically Activated Cation Channels. *Science* (1979) **330**, 55–60 (2010).
16. Coste, B. et al. Piezo proteins are pore-forming subunits of mechanically activated channels. *Nature* **483**, 176–181 (2012).
17. Rode, B. et al. Piezo1 channels sense whole body physical activity to reset cardiovascular homeostasis and enhance performance. *Nat. Commun.* **8**, 350 (2017).
18. Shi, J. et al. Sphingomyelinase Disables Inactivation in Endogenous PIEZO1 Channels. *Cell Rep.* **33**, 108225 (2020).
19. Little, T. L., Xia, J. & Duling, B. R. Dye Tracers Define Differential Endothelial and Smooth Muscle Coupling Patterns Within the Arteriolar Wall. *Circ. Res* **76**, 498–504 (1995).
20. Emerson, G. G., Segal, S. S., The John, F. B. & John, T. B. Electrical Coupling Between Endothelial Cells and Smooth Muscle Cells in Hamster Feed Arteries. *Circ. Res* **87**, 474–479 (2000).
21. Saunders, A. et al. Molecular Diversity and Specializations among the Cells of the Adult Mouse Brain. *Cell* **174**, 1015–1030.e16 (2018).
22. Vanlandewijck, M. et al. A molecular atlas of cell types and zonation in the brain vasculature. *Nature* **554**, 475–480 (2018).
23. Chi, S. et al. Astrocytic Piezo1-mediated mechanotransduction determines adult neurogenesis and cognitive functions. *Neuron* **110**, 2984–2999.e8 (2022).
24. Hu, J. et al. Microglial Piezo1 senses Aβ fibril stiffness to restrict Alzheimer’s disease. *Neuron* **111**, 15–29.e8 (2023).
25. Ma, S. et al. Common PIEZO1 Allele in African Populations Causes RBC Dehydration and Attenuates Plasmodium Infection. *Cell* **173**, 443–455.e12 (2018).
26. Albuissou, J. et al. Dehydrated hereditary stomatocytosis linked to gain-of-function mutations in mechanically activated PIEZO1 ion channels. *Nat. Commun.* **4**, 1–9 (2013).
27. Wenzel, J. et al. The SARS-CoV-2 main protease Mpro causes microvascular brain pathology by cleaving NEMO in brain endothelial cells. *Nat. Neurosci.* **24**, 1522–1533 (2021).
28. Brown, W. R. A review of string vessels or collapsed, empty basement membrane tubes. *J. Alzheimers Dis.* **21**, 725–739 (2010).
29. Gao, X. et al. Reduction of neuronal activity mediated by blood-vessel regression in the brain. <https://doi.org/10.1101/2020.09.15.262782>. (2020).
30. Holt, J. R. et al. Spatiotemporal dynamics of PIEZO1 localization controls keratinocyte migration during wound healing. *Elife* **10**, e65415 (2021).
31. Kang, H. M. et al. Optical measurement of mouse strain differences in cerebral blood flow using indocyanine green. *J. Cereb. Blood Flow. Metab.* **35**, 912–916 (2015).
32. Barone, F. C., Knudsen, D. J., Nelson, A. H., Feuerstein, G. Z. & Willette, R. N. Mouse strain differences in susceptibility to cerebral ischemia are related to cerebral vascular anatomy. *J. Cereb. Blood Flow. Metab.* **13**, 683–692 (1993).
33. Wang, S. et al. Endothelial cation channel PIEZO1 controls blood pressure by mediating flow-induced ATP release. *J. Clin. Investig.* **126**, 4527–4536 (2016).
34. Wenzel, J. et al. Impaired endothelium-mediated cerebrovascular reactivity promotes anxiety and respiration disorders in mice. *Proc. Natl Acad. Sci.* **117**, 1753–1761 (2020).
35. Ridder, D. A. et al. TAK1 in brain endothelial cells mediates fever and lethargy. *J. Exp. Med* **208**, 2615 (2011).
36. Hosford, P. S. et al. CO<sub>2</sub> signaling mediates neurovascular coupling in the cerebral cortex. *Nat. Commun.* **13**, 1–11 (2022).
37. Tournissac, M. et al. Neurovascular coupling and CO<sub>2</sub> interrogate distinct vascular regulations. *Nat. Commun.* **15**, 7635 (2024).
38. Iadecola, C. et al. Vascular Cognitive Impairment and Dementia: JACC Scientific Expert Panel. *J. Am. Coll. Cardiol.* **73**, 3326–3344 (2019).
39. Santisteban, M. M., Iadecola, C. & Carnevale, D. Hypertension, Neurovascular Dysfunction, and Cognitive Impairment. *Hypertension* **80**, 22–34 (2022).
40. Toth, P., Tarantini, S., Csiszar, A. & Ungvari, Z. Functional vascular contributions to cognitive impairment and dementia: Mechanisms and consequences of cerebral autoregulatory dysfunction, endothelial impairment, and neurovascular uncoupling in aging. *Am. J. Physiol. Heart Circulat. Physiol.* **312**, H1–H20 (2017).
41. Iadecola, C. The overlap between neurodegenerative and vascular factors in the pathogenesis of dementia. *Acta Neuropathologica* **2010** 120:3 **120**, 287–296 (2010).
42. Snyder, H. M. et al. Vascular contributions to cognitive impairment and dementia including Alzheimer’s disease. *Alzheimer’s Dement.* **11**, 710–717 (2015).
43. Tarantini, S. et al. Pharmacologically-induced neurovascular uncoupling is associated with cognitive impairment in mice. *J. Cereb. Blood Flow. Metab.* **35**, 1871–1881 (2015).
44. Koizumi, K. et al. Apoε4 disrupts neurovascular regulation and undermines white matter integrity and cognitive function. *Nat. Commun.* **9**, 1–11 (2018).
45. Antunes, M. & Biala, G. The novel object recognition memory: neurobiology, test procedure, and its modifications. *Cogn. Process* **13**, 93–110 (2012).

46. d'Isa, R., Comi, G. & Leocani, L. Apparatus design and behavioural testing protocol for the evaluation of spatial working memory in mice through the spontaneous alternation T-maze. *Sci. Rep.* **11**, 21177 (2021).
47. Nippert, A. R., Biesecker, K. R. & Newman, E. A. Mechanisms Mediating Functional Hyperemia in the Brain. *Neuroscientist* **24**, 73–83 (2018).
48. Ranade, S. et al. Piezo1, a mechanically activated ion channel, is required for vascular development in mice. *Proc. Natl Acad. Sci.* **111**, 10347–10352 (2014).
49. Li, J. et al. Piezo1 integration of vascular architecture with physiological force. *Nature* **515**, 279–282 (2014).
50. Longden, T. A. et al. Local IP<sub>3</sub> receptor-mediated Ca<sup>2+</sup> signals compound to direct blood flow in brain capillaries. *Sci. Adv.* **7**, eabh0101 (2021).
51. Ottolini, M. et al. Mechanisms underlying selective coupling of endothelial Ca<sup>2+</sup> signals with eNOS vs. IK/SK channels in systemic and pulmonary arteries. *J. Physiol.* **598**, 3577–3596 (2020).
52. Zhang, L., Papadopoulos, P. & Hamel, E. Endothelial TRPV4 channels mediate dilation of cerebral arteries: impairment and recovery in cerebrovascular pathologies related to Alzheimer's disease. *Br. J. Pharm.* **170**, 661–670 (2013).
53. Kalucka, J. et al. Single-Cell Transcriptome Atlas of Murine Endothelial Cells. *Cell* **180**, 764–779.e20 (2020).
54. Mulligan, S. J. & MacVicar, B. A. Calcium transients in astrocyte endfeet cause cerebrovascular constrictions. *Nature* **431**, 195–199 (2004).
55. Bucher, E. S. et al. Medullary norepinephrine neurons modulate local oxygen concentrations in the bed nucleus of the stria terminalis. *J. Cereb. Blood Flow. Metab.* **34**, 1128–1137 (2014).
56. Kim, K. J., Diaz, J. R., Iddings, J. A. & Filosa, J. A. Vasculo-Neuronal Coupling: Retrograde Vascular Communication to Brain Neurons. *J. Neurosci.* **36**, 12624–12639 (2016).
57. Macvicar, B. A. & Newman, E. A. Astrocyte Regulation of Blood Flow in the Brain. *Cold Spring Harb. Perspect. Biol.* **7**, 1–15 (2015).
58. Chen, B. R., Kozberg, M. G., Bouchard, M. B., Shaik, M. A. & Hillman, E. M. C. A Critical Role for the Vascular Endothelium in Functional Neurovascular Coupling in the Brain. *J. Am. Heart Assoc.* **3**, e000787 (2014).
59. Lim, X. R. & Harraz, O. F. Mechanosensing by Vascular Endothelium. *Annu. Rev. Physiol.* **86**, 71–97 (2024).
60. Pyke, K. E. & Tschakovsky, M. E. The relationship between shear stress and flow-mediated dilatation: implications for the assessment of endothelial function. *J. Physiol.* **568**, 357–369 (2005).
61. Toth, P., Rozsa, B., Springo, Z., Doczi, T. & Koller, A. Isolated human and rat cerebral arteries constrict to increases in flow: role of 20-HETE and TP receptors. *J. Cereb. Blood Flow. Metab.* **31**, 2096–2105 (2011).
62. Craig, J. & Martin, W. Dominance of flow-mediated constriction over flow-mediated dilatation in the rat carotid artery. *Br. J. Pharm.* **167**, 527–536 (2012).
63. Schaller, B. & Graf, R. Different compartments of intracranial pressure and its relationship to cerebral blood flow. *J. Trauma* **59**, 1521–1531 (2005).
64. Thorin-Trescases, N. & Bevan, J. A. High Levels of Myogenic Tone Antagonize the Dilator Response to Flow of Small Rabbit Cerebral Arteries. *Stroke* **29**, 1194–1201 (1998).
65. Ngai, A. C. & Winn, H. R. Modulation of Cerebral Arteriolar Diameter by Intraluminal Flow and Pressure. *Circ. Res.* **77**, 832–840 (1995).
66. Garcia-Roldan, J. L. & Bevan, J. A. Flow-induced constriction and dilation of cerebral resistance arteries. *Circ. Res.* **66**, 1445–1448 (1990).
67. Benson, J. C., Madhavan, A. A., Cutsforth-Gregory, J. K., Johnson, D. R. & Carr, C. M. The Monro-Kellie Doctrine: A Review and Call for Revision. *AJNR Am. J. Neuroradiol.* **44**, 2–6 (2023).
68. Chen, Q. et al. Haemodynamics-driven developmental pruning of brain vasculature in zebrafish. *PLoS Biol.* **10**, e1001374 (2012).
69. Gibson, G. E. & Duffy, T. E. Impaired synthesis of acetylcholine by mild hypoxic hypoxia or nitrous oxide. *J. Neurochem.* **36**, 28–33 (1981).
70. Matrongolo, M. J. et al. Piezo1 agonist restores meningeal lymphatic vessels, drainage, and brain-CSF perfusion in craniosynostosis and aged mice. *J. Clin. Invest.* **134**, e171468 (2023).
71. Moore, C. I. & Cao, R. The hemo-neural hypothesis: On the role of blood flow in information processing. *J. Neurophysiol.* **99**, 2035–2047 (2008).
72. Velasco-Estevéz, M., Rolle, S. O., Mampay, M., Dev, K. K. & Sheridan, G. K. Piezo1 regulates calcium oscillations and cytokine release from astrocytes. *Glia* **68**, 145–160 (2020).
73. Zhu, J. et al. The mechanosensitive ion channel Piezo1 contributes to ultrasound neuromodulation. *Proc. Natl. Acad. Sci. USA* **120**, (2023).
74. Garcia, V. et al. PIEZO1 expression at the glio-vascular unit adjusts to neuroinflammation in seizure conditions. *Neurobiol Dis* **187**, 106297 (2023).
75. Wang, C. et al. Hippocampus–Prefrontal Coupling Regulates Recognition Memory for Novelty Discrimination. *J. Neurosci.* **41**, 9617–9632 (2021).
76. Tanimizu, T., Kono, K. & Kida, S. Brain networks activated to form object recognition memory. *Brain Res Bull.* **141**, 27–34 (2018).
77. Deacon, R. M. J. & Rawlins, J. N. P. T-maze alternation in the rodent. *Nat. Protoc.* **1**, 7–12 (2006).
78. Shaw, K. et al. Neurovascular coupling and oxygenation are decreased in hippocampus compared to neocortex because of microvascular differences. *Nat. Commun.* **12**, 1–16 (2021).
79. Malek, A. M., Alper, S. L. & Izumo, S. Hemodynamic Shear Stress and Its Role in Atherosclerosis. *JAMA* **282**, 2035–2042 (1999).
80. Cecchi, E. et al. Role of hemodynamic shear stress in cardiovascular disease. *Atherosclerosis* **214**, 249–256 (2011).
81. Martin-Almedina, S., Mansour, S. & Ostergaard, P. Human phenotypes caused by *PIEZO1* mutations; one gene, two overlapping phenotypes? *J. Physiol.* **596**, 985–992 (2018).
82. Lukacs, V. et al. Impaired PIEZO1 function in patients with a novel autosomal recessive congenital lymphatic dysplasia. *Nat. Commun.* **6**, 1–7 (2015).
83. Nguetse, C. N. et al. A common polymorphism in the mechanosensitive ion channel PIEZO1 is associated with protection from severe malaria in humans. *Proc. Natl Acad. Sci. USA* **117**, 9074–9081 (2020).
84. Nakamichi, R. et al. The mechanosensitive ion channel PIEZO1 is expressed in tendons and regulates physical performance. *Sci. Transl. Med.* **14**, 5557 (2022).
85. Hill, R. Z., Loud, M. C., Dubin, A. E., Peet, B. & Patapoutian, A. PIEZO1 transduces mechanical itch in mice. *Nature* **607**, 104–110 (2022).
86. Koide, M. et al. Differential restoration of functional hyperemia by antihypertensive drug classes in hypertension-related cerebral small vessel disease. *J. Clin. Invest.* **131**, e149029 (2021).
87. Capone, C. et al. Mechanistic insights into a TIMP3-sensitive pathway constitutively engaged in the regulation of cerebral hemodynamics. *Elife* **5**, e17536 (2016).
88. Staehr, C. et al. Abnormal neurovascular coupling as a cause of excess cerebral vasodilation in familial migraine. *Cardiovasc Res* **116**, 2009–2020 (2020).
89. Lee, B., Sosnovtseva, O., Sørensen, C. M. & Postnov, D. D. Multi-scale laser speckle contrast imaging of microcirculatory vasoreactivity. *Biomed. Opt. Express* **13**, 2312 (2022).
90. González Olmos, A., Zilpelwar, S., Sunil, S., Boas, D. A. & Postnov, D. D. Optimizing the precision of laser speckle contrast imaging. *Sci. Rep.* **13**, 17970 (2023).

91. Sunil, S., Zilpelwar, S., Boas, D. A. & Postnov, D. D. Guidelines for obtaining an absolute blood flow index with laser speckle contrast imaging. <https://doi.org/10.1101/2021.04.02.438198> (2021).
92. Postnov, D. D., Cheng, X., Erdener, S. E. & Boas, D. A. Choosing a laser for laser speckle contrast imaging. *Sci. Rep.* **9**, 1–6 (2019).
93. Postnov, D. D., Akther, S. & Mikkelsen, M. B. Choosing a polarisation configuration for dynamic light scattering and laser speckle contrast imaging. *Biomed. Opt. Express* **15**, 336–345 (2024).
94. Boas, D. A. & Dunn, A. K. Laser speckle contrast imaging in biomedical optics. *J. Biomed. Opt.* **15**, 011109 (2010).
95. Hariharan, A., Robertson, C. D., Garcia, D. C. G. & Longden, T. A. Brain capillary pericytes are metabolic sentinels that control blood flow through a KATP channel-dependent energy switch. *Cell Rep.* **41**, 111872 (2022).
96. Ridder, D. A. et al. Brain endothelial TAK1 and NEMO safeguard the neurovascular unit. *J. Exp. Med.* **212**, 1529–1549 (2015).

## Acknowledgements

We thank Dr. Ardem Patapoutian for generously sharing the Piezo1<sup>cx/cx</sup> mice, Dr. Mark Nelson for support and valuable discussions, Dan Enders, Theresa Wellman (University of Vermont), and Beate Lembrich (University of Lübeck) for technical assistance. OFH was supported by the National Heart, Lung, and Blood Institute (R01HL169681), the National Institute on Aging (R21AG082193), the National Institute of General Medical Sciences (P20GM135007), the American Heart Association (20CDA35310097), the Bloomfield Early Career Professorship in Cardiovascular Research, the Totman Medical Research Trust, the Larner College of Medicine, University of Vermont, and the Cardiovascular Research Institute of Vermont. This project has been made possible in part by grant 2024-338506 (to OFH and TAL) from the Chan Zuckerberg Initiative DAF, an advised fund of Silicon Valley Community Foundation. MK was supported by the National Institute of General Medical Sciences (P20GM135007). The authors acknowledge the support and guidance of the staff and investigators of the Vermont Center for Cardiovascular and Brain Health, supported by the National Institute of General Medical Sciences (P20GM135007). TAL was supported by the National Institute on Aging and National Institute of Neurological Disorders and Stroke (1R01AG066645, 5R01NS115401, and 1DP2NS121347-01), NW was supported by the American Heart Association (23POST1023086) and AH was supported by the American Heart Association and the D.C. Women's Board (Award 830093). JW was supported by the Deutsche Forschungsgemeinschaft (WE 6456/1-1 and GRK1957), and JMS was supported by the National Institute on Alcohol Abuse and Alcoholism (R00AA024837) and a pilot project award through U54GM115516. DDP was supported by Lundbeck Foundation (R345-2020-1782).

## Author contributions

O.F.H. conceived and designed the study. X.R.L. (equal), M.M.A.-A. (equal), M.L., M. K., A.J.S., A.H., N.W., T.A.L., K.A.L., J.M.S., D.Z., J.W. and O.F.H. performed experiments and data analysis. D.D.P. helped establish LSCI methods and analysis, and C.P. helped with the optimization of LSCI data analysis. M.S. and J.W. helped establish brain endothelial cell specific mouse models. O.F.H. wrote the original and revised manuscript with input from T.A.L., J.M.S., J.W., and D.D.P. All authors reviewed and approved the final version of the manuscript.

## Competing interests

The authors declare no competing interests.

## Additional information

**Supplementary information** The online version contains supplementary material available at <https://doi.org/10.1038/s41467-024-52969-0>.

**Correspondence** and requests for materials should be addressed to Osama F. Harraz.

**Reprints and permissions information** is available at <http://www.nature.com/reprints>

**Publisher's note** Springer Nature remains neutral with regard to jurisdictional claims in published maps and institutional affiliations.

**Open Access** This article is licensed under a Creative Commons Attribution-NonCommercial-NoDerivatives 4.0 International License, which permits any non-commercial use, sharing, distribution and reproduction in any medium or format, as long as you give appropriate credit to the original author(s) and the source, provide a link to the Creative Commons licence, and indicate if you modified the licensed material. You do not have permission under this licence to share adapted material derived from this article or parts of it. The images or other third party material in this article are included in the article's Creative Commons licence, unless indicated otherwise in a credit line to the material. If material is not included in the article's Creative Commons licence and your intended use is not permitted by statutory regulation or exceeds the permitted use, you will need to obtain permission directly from the copyright holder. To view a copy of this licence, visit <http://creativecommons.org/licenses/by-nc-nd/4.0/>.

© The Author(s) 2024